Supporting information for: Imaging Time-Dependent Electronic Currents Through a Graphene-Based Nanojunction

Vincent Pohl,[†,‡] Lukas Eugen Marsoner Steinkasserer,[‡] and Jean Christophe Tremblay[*,¶]

† *Quantum on Demand, c/o Freie Universität Berlin, Altensteinstr. 40, 14195 Berlin, Germany*

‡ *Institut für Chemie und Biochemie, Freie Universität Berlin, Takustr. 3, 14195 Berlin, Germany*

¶ *Laboratoire de Physique et Chimie Théoriques, CNRS-Université de Lorraine, UMR 7019, ICPM, 1 Bd Arago, 57070 Metz, France*

E-mail: jean-christophe.tremblay@univ-lorraine.fr

Review of the Driven Liouville-von-Neumann Equation

Within the framework of the driven Liouville-von-Neumann (DLvN) approach for time-dependent electronic transport simulations, a finite molecular junction is formally divided into three parts: the left lead (L), the extended molecule (M), and the right lead (R) (cf.

Fig. S1). In the localized representation, the time-evolution of the system is described by[S1–S3]

$$\begin{aligned}\frac{\partial \underline{\underline{\rho}}(t)}{\partial t} &= -\frac{\imath}{\hbar}\left[\underline{\underline{H}}_{\mathrm{sys}}, \underline{\underline{\rho}}(t)\right] - \frac{\imath}{\hbar}\left[\imath\underline{\underline{W}}, \underline{\underline{\rho}}(t)\right]_+ \\ &= -\frac{\imath}{\hbar}\left[\underline{\underline{H}}_{\mathrm{sys}}, \underline{\underline{\rho}}(t)\right] - \frac{1}{2\hbar}\begin{pmatrix} \left[\underline{\underline{\Gamma}}_{\mathrm{L}}, \left(\underline{\underline{\rho}}_{\mathrm{L}}(t) - \underline{\underline{\rho}}^{0}_{\mathrm{L}}\right)\right]_+ & \underline{\underline{\Gamma}}_{\mathrm{L}}\underline{\underline{\rho}}_{\mathrm{LM}}(t) & \underline{\underline{\Gamma}}_{\mathrm{L}}\underline{\underline{\rho}}_{\mathrm{LR}}(t) + \underline{\underline{\rho}}_{\mathrm{LR}}(t)\underline{\underline{\Gamma}}_{\mathrm{R}} \\ \underline{\underline{\rho}}_{\mathrm{ML}}(t)\underline{\underline{\Gamma}}_{\mathrm{L}} & 0 & \underline{\underline{\rho}}_{\mathrm{MR}}(t)\underline{\underline{\Gamma}}_{\mathrm{R}} \\ \underline{\underline{\Gamma}}_{\mathrm{R}}\underline{\underline{\rho}}_{\mathrm{RL}}(t) + \underline{\underline{\rho}}_{\mathrm{RL}}(t)\underline{\underline{\Gamma}}_{\mathrm{L}} & \underline{\underline{\Gamma}}_{\mathrm{R}}\underline{\underline{\rho}}_{\mathrm{RM}}(t) & \left[\underline{\underline{\Gamma}}_{\mathrm{R}}, \left(\underline{\underline{\rho}}_{\mathrm{R}}(t) - \underline{\underline{\rho}}^{0}_{\mathrm{R}}\right)\right]_+ \end{pmatrix}, \end{aligned} \tag{S1}$$

where $\hbar$ is the reduced Planck constant, $\underline{\underline{\rho}}(t)$ is the one-particle reduced density matrix, and $\underline{\underline{H}}_{\mathrm{sys}}$ refers to the system's Hamiltonian. The diagonal matrix $\underline{\underline{\rho}}^{0}_{\ell}$ describes the equilibrium Fermi-Dirac statistics of the respective lead $\ell = \{\mathrm{L}, \mathrm{R}\}$,

$$f_\ell\big(\varepsilon^\ell_a\big) = \frac{1}{\exp\left[(\varepsilon^\ell_a - \mu_\ell)/k_{\mathrm{B}}T_\ell\right] + 1} \tag{S2}$$

with the Boltzmann constant k_{B}, the lead state energies ε^ℓ_a, the electronic temperature T_ℓ, and the chemical potential μ_ℓ. While the first term on the right-hand side of Eq. (S1) describes the coherent time-evolution of the system, the second term containing the complex Hamiltonian $\imath\underline{\underline{W}}$ is driving the system dynamically towards a non-equilibrium situation at a rate $\underline{\underline{\Gamma}}_\ell/\hbar$. This term can be attributed to the coupling of the finite lead section to an implicit semi-infinite electronic reservoir within the wide-band approximation.[S3] It is often defined as a constant factor that is either adjusted to the reflection time scales in a finite junction model,[S4] or fitted to a NEGF reference calculation.[S2,S5,S6] Recently, the DLvN approach has been extended to parameter-free state-dependent broadening factors that allow for a more accurate description of the couplings between the finite lead section and the electronic reservoir.[S3] This is the approach we choose to follow in the present work, and we will review the procedure below.

The influence of a semi-infinite reservoir on a finite lead section is described by the

reservoir's retarded self-energy matrix

$$\underline{\underline{\Sigma}}^{r}_{\mathrm{res}}(\varepsilon) = \left(\epsilon^{+}\,\underline{\underline{S}}_{\ell,\mathrm{res}} - \underline{\underline{V}}_{\ell,\mathrm{res}}\right)\underline{\underline{G}}^{r,0}_{\mathrm{res}}(\epsilon^{+})\left(\epsilon^{+}\,\underline{\underline{S}}_{\mathrm{res},\ell} - \underline{\underline{V}}_{\mathrm{res},\ell}\right) \tag{S3}$$

where $S_{\ell,\mathrm{res}}$ is the overlap between a lead and the reservoir, $V_{\ell,\mathrm{res}}$ is the corresponding coupling matrix, and $\epsilon^{+} = \epsilon + \imath\eta$ with $\eta \to 0^{+}$. The retarded surface Green's function of the isolated reservoir is given by

$$\underline{\underline{G}}^{r,0}_{\mathrm{res}}(\varepsilon) = \left[\epsilon^{+}\,\underline{\underline{S}}_{\mathrm{res}} - \underline{\underline{H}}^{0}_{\mathrm{res}}\right]^{-1} \tag{S4}$$

with the Hamiltonian matrix of the uncoupled semi-infinite reservoir $\underline{\underline{H}}^{0}_{\mathrm{res}}$ and the overlap matrix $\underline{\underline{S}}_{\mathrm{res}}$. For each lead state $\left|\varphi^{\ell}_{a}\right\rangle$, a dressed Hamiltonian is constructed by adding the reservoir's self-energy evaluated at the energy of the respective lead eigenenergy, $\underline{\underline{\Sigma}}^{r}_{\mathrm{res}}(\varepsilon^{\ell}_{a})$, to the lead Hamiltonian $\underline{\underline{H}}_{\ell}$. A subsequent diagonalization of this new Hamiltonian matrix, yields new dressed eigenstates and eigenenergies. By gradually turning on $\underline{\underline{\Sigma}}^{r}_{\mathrm{res}}(\varepsilon^{\ell}_{a})$, it is possible to follow a given state of the undressed Hamiltonian. In matrix notation, the dressed eigenvector corresponding to the undressed state $\left|\varphi^{\ell}_{a}\right\rangle$ reads

$$\left(\underline{\underline{H}}_{\ell} + \underline{\underline{\Sigma}}^{r}_{\mathrm{res}}(\varepsilon^{\ell}_{a})\right)\underline{\underline{U}}_{\ell_a} = \underline{\underline{U}}_{\ell_a}\underline{\underline{\Lambda}}_{\ell_a}, \tag{S5}$$

The level broadening $\underline{\underline{\Gamma}}^{(a,a)}_{\ell}$ caused by the finite life time of this state is given by the imaginary part of the dressed eigenvalue[S3,S7,S8]

$$\underline{\underline{\Gamma}}^{(a,a)}_{\ell} = -2\,\mathrm{Im}\left\{\underline{\underline{\Lambda}}_{\ell_a}\right\}^{(a,a)} \tag{S6}$$

Construction of the Atomistic Model

Fig. S1 (upper panel) shows a sketch of the finite model system used in this work, with the three parts highlighted as colored areas. In contrast to previous studies, the starting point

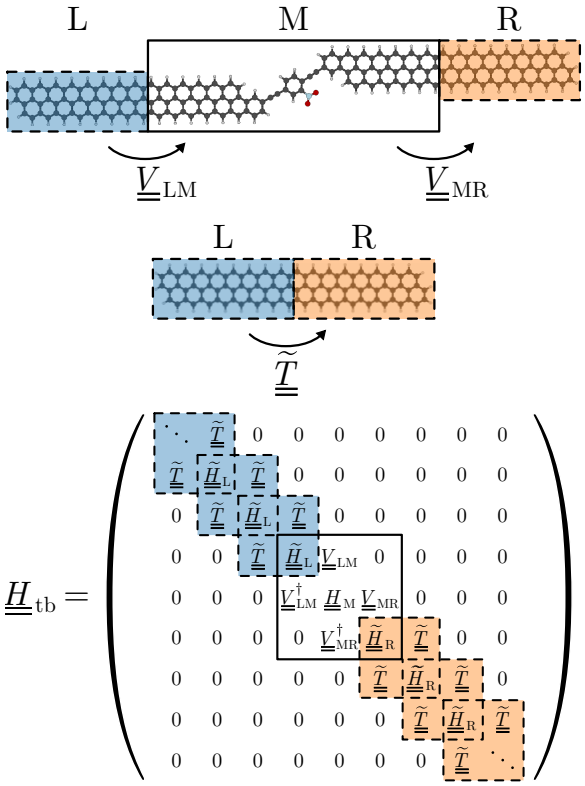

Figure S1: Same as Fig. 1 of the main manuscript. Upper panel: Ball-and-sticks representation of the finite OPE-GNR model system used within the work. The nanojunction is divided into three parts: the left lead (L, in blue), the extended molecule (M, black solid box), and the right lead (R, in orange). Central panel: Ball-and-sticks representation of the lead dimer composed of a left lead part (L, in blue) and a right lead part (R, in orange). Bottom panel: Conceptual sketch of the different contributions to the tight-binding Hamiltonian matrix $\underline{\underline{H}}_{\mathrm{tb}}$. This Hamiltonian is parametrized by localizing the molecule's (upper panel) molecular orbitals onto the three parts of the device, and extending the leads using the matrix elements of the dimer (central panel). The tilde denotes matrix blocks obtained from the lead dimer calculation.

for the localization procedure is an orthonormal set of molecular orbitals for the entire finite model system (MOs) $\{|\varphi_a\rangle\}_{n_{\mathrm{MO}}}$ and their corresponding eigenenergies $\vec{\varepsilon} = \{\varepsilon_a\}_{n_{\mathrm{MO}}}$. These are obtained from a ground state density functional theory (DFT) calculation, which satisfy a one-electron Kohn-Sham equation of the form

$$\hat{h}_{\mathrm{KS}} |\varphi_a\rangle = \varepsilon_a |\varphi_a\rangle \tag{S7}$$

with the Hamiltonian $\hat{h}_{\mathrm{KS}} = -\frac{\hbar^2}{2m_e}\nabla_e^2 + \hat{v}_{\mathrm{KS}}$, where m_e is the mass of an electron and $\hat{v}_{\mathrm{KS}}$ is the Kohn-Sham potential operator. For molecular systems composed of N_α atoms, MOs are usually expanded in a finite set of atom-centered orbitals (AOs)

$$\varphi_a(\vec{r}) = \sum_{\alpha=1}^{N_\alpha} \sum_{i_\alpha=1}^{n_{\mathrm{AO}}(\alpha)} D_{i_\alpha}^{(a)} \chi_{i_\alpha}(\vec{r} - \vec{R}_\alpha), \tag{S8}$$

where $\vec{r}$ and $\vec{R}_\alpha$ are the coordinates of an electron and of nucleus α, respectively. The index $n_{\mathrm{AO}(\alpha)}$ defines the number of AOs, $\chi_{i_\alpha}(\vec{r} - \vec{R}_\alpha)$, centered on atom α.

Modern theoretical approaches to electronic transport, such as non-equilibrium Green's functions and the DLvN ansatz, describe the dynamics of electrons in terms of pseudo-spectral states localized on different parts of the nanojunction: two leads, and the scattering region. Since the MOs obtained from a ground state quantum chemistry calculations are generally delocalized over the whole extent of the nanostructure, localization onto each of the three sections is required. In the present work, this is achieved by following a sequential procedure involving numerical unitary basis set transformations of a selected subset of MOs within a specific energy window. This bottom-up approach drastically reduces the basis size while conserving the orthogonality of the MOs obtained from conventional quantum chemistry calculations. Note that in previous implementations,[S2–S6] the localized states of the three segments are defined from the atomic basis functions of the atoms belonging to the different sites of the junctions. As a consequence, it is not possible to reduce the basis set size by choosing only basis functions within the energy region of interest.

Defining Localized Lead States

To first define a set of localized lead states, we construct a lead dimer, as depicted in Fig. S1 (central panel). This prevents any artificial influence of the asymmetry of central group on

the leads. The one-electron Kohn-Sham equation of this dimer is given by

$$\hat{h}_{\mathrm{KS}} \left|\widetilde{\varphi}_a\right\rangle = \widetilde{\varepsilon}_a \left|\widetilde{\varphi}_a\right\rangle . \tag{S9}$$

For clarity, all matrices represented in the MO basis of the lead dimer are denoted with a tilde. Note that the primitive atomic orbital basis and the relative position of the lead atoms are identical to those of the complete system (cf. Fig. S1 (upper panel)). In order to localize the MOs on the dimer units, a linear operator quantifying the differential projection on the right and left leads is used to define a linear metric as

$$\big(\underline{\underline{\widetilde{R}}} - \underline{\underline{\widetilde{L}}}\big)\underline{\underline{\widetilde{Q}}} = \underline{\underline{\widetilde{Q}}}\,\widetilde{\Lambda}_{\mathrm{RL}} \tag{S10}$$

where

$$\begin{aligned} \underline{\underline{\widetilde{L}}}_{ab} &= \left\langle \widetilde{\varphi}_a \middle| \hat{P}_{\mathrm{L}} \middle| \widetilde{\varphi}_b \right\rangle \\ &= \sum_{\substack{\alpha \\ \beta\in\{\mathrm{L}\}}} \sum_{\substack{i_\alpha \\ j_\beta}} \widetilde{D}^{(a)}_{i_\alpha} \widetilde{D}^{(b)}_{j_\beta} \left\langle \widetilde{\chi}_{i_\alpha} \middle| \widetilde{\chi}_{j_\beta} \right\rangle , \end{aligned} \tag{S11}$$

and accordingly

$$\underline{\underline{\widetilde{R}}}_{ab} = \sum_{\substack{\alpha \\ \beta\in\{\mathrm{R}\}}} \sum_{\substack{i_\alpha \\ j_\beta}} \widetilde{D}^{(a)}_{i_\alpha} \widetilde{D}^{(b)}_{j_\beta} \left\langle \widetilde{\chi}_{i_\alpha} \middle| \widetilde{\chi}_{j_\beta} \right\rangle . \tag{S12}$$

Here, $\hat{P}_{\mathrm{L/R}}$ is the Mulliken projector onto the atoms of the left or right lead, respectively. The spectrum of the operator $(\underline{\underline{\widetilde{R}}} - \underline{\underline{\widetilde{L}}})$ gives a measure of the localization of the MOs on the leads. The eigenvalues $\widetilde{\Lambda}_{\mathrm{RL}} < 0$ correspond to a localization onto the left lead (blue shaded area in the central panel of Fig. S1), and $\widetilde{\Lambda}_{\mathrm{RL}} > 0$ to a localization onto the right lead (orange shaded area in Fig. S1). To avoid artificial mixing between energetically widely separated states, an energy weighting, $\exp\big(-(\epsilon_a - \epsilon_b)^2/2\sigma^2\big)$ with $\sigma = 1\,\mathrm{eV}$, has been applied to the coefficients in Eq. (S10). Note that the simulation results do not depend strongly on the choice of energy window, only the locality of the molecular orbitals and the number of coupling partners through the junction are affected. Without energy window, the MOs become more localized

in space but are more delocalized in energy. Hence the stronger mixing accross the junction. Fortunately, this only influences the convergence of the basis used for the DLvN simulations, but not the overall dynamics. The Gaussian energy weighting width is chosen to keep the MO basis small but still well localized. Subsequent diagonalization of the resulting diagonal blocks of the Hamiltonian yields a new pseudo-spectral basis $\left\{\left|\widetilde{\psi}_{a}^{\mathrm{L/R}}\right\rangle\right\}_{n_{\mathrm{L}}\equiv n_{\mathrm{R}}}$, where the Hamiltonian takes the form

$$\underline{\underline{\widetilde{h}}}_{\mathrm{dimer}} = \begin{pmatrix} \underline{\underline{\widetilde{H}}}_{\mathrm{L}} & \underline{\underline{\widetilde{T}}} \\ \underline{\underline{\widetilde{T}}}^{\dagger} & \underline{\underline{\widetilde{H}}}_{\mathrm{R}} \end{pmatrix}. \tag{S13}$$

After adjusting the phase of the lead basis functions, i.e., imposing $\left\langle \widetilde{\psi}_{a}^{\mathrm{L}} \middle| \widetilde{\psi}_{b}^{\mathrm{R}} \right\rangle \stackrel{!}{=} \delta_{a,b}$ after aligning the atoms of the left and right lead units, the matrix elements in Eq. (S13) obey the symmetry relations $\underline{\underline{\widetilde{H}}}_{\mathrm{L}} \equiv \underline{\underline{\widetilde{H}}}_{\mathrm{R}}$ and $\underline{\underline{\widetilde{T}}} \equiv \underline{\underline{\widetilde{T}}}^{\dagger}$. That is, in energy space, the left and the right lead are equivalent. Further, the diagonal blocks $\underline{\underline{\widetilde{H}}}_{\mathrm{L/R}}$ of the Hamiltonian are diagonal, with their entries containing the associated eigenvalues.

Now, the eigenfunctions of the dimer can be transformed to the original system basis (cf. Eq. (S7)) using the resolution-of-identity

$$\left|\psi_{a}^{\mathrm{L/R}}\right\rangle = \sum_{b}^{n_{\mathrm{MO}}} \left|\varphi_{b}\right\rangle \underline{\underline{U}}_{\mathrm{L/R}}^{(b,a)} \tag{S14}$$

$$\underline{\underline{U}}_{\mathrm{L/R}}^{(b,a)} = \left\langle \varphi_{b} \middle| \widetilde{\psi}_{a}^{\mathrm{L/R}} \right\rangle \tag{S15}$$

To ensure that subsequent quantum dynamics simulations remain computationally tractable, we choose to retain only subsets of $n_{\mathrm{L/R}}$ lead states and n_{MO} molecular orbitals within a symmetric energy window around the Fermi energy.[S2] This gives rise to two convergence parameters: the energy range ΔE_{lead} for choosing the lead basis functions, $n_{\mathrm{L/R}}$, and the energy range $\Delta E_{\mathrm{basis}}$ for choosing the basis set size of the complete system, n_{MO}. The convergence of the dynamics with respect to these two parameters is benchmarked in the next section. This procedure allows defining two transformation matrices for the left and right localized lead states, $\underline{\underline{U}}_{\mathrm{L/R}}$, with elements given by Eq. (S15).

Defining Localized States of the Extended Molecule

As a final step towards the construction of the localized Hamiltonian, the extended molecule (M) pseudo-spectral basis functions are localized according to the linear metric

$$\big(\underline{\underline{1}} - \underline{\underline{R}} - \underline{\underline{L}}\big)\underline{\underline{Q}}_{\mathrm{M}} = \underline{\underline{Q}}_{\mathrm{M}}\Lambda_{\mathrm{M}} \tag{S16}$$

The projectors are defined as in Eq. (S10), but the matrix elements are computed using the delocalized MOs of the complete device model and not those of the dimer. The $n_{\mathrm{L/R}}$ eigenfunctions associated with the smallest eigenvalues can be assigned to the left and right leads. The remaining $n_{\mathrm{M}} = (n_{\mathrm{MO}} - n_{\mathrm{R}} - n_{\mathrm{L}})$ largest eigenvalues Λ_{M} are attributed to the extended molecule. Diagonalization of the associated $n_{\mathrm{M}} \times n_{\mathrm{M}}$ Hamiltonian matrix allows defining a last transformation matrix as

$$\underline{\underline{h}}_{\mathrm{M}}\underline{\underline{U}}_{\mathrm{M}} = \underline{\underline{U}}_{\mathrm{M}}\underline{\underline{H}}_{\mathrm{M}} \tag{S17}$$

where the matrix $\underline{\underline{H}}_{\mathrm{M}}$ contains the eigenvalues of the extended molecule pseudo-spectral basis functions. The Hamiltonian of the finite nanojunction model in the localized pseudo spectral basis can be obtained by transforming the eigenvalue matrix of the extended system, $\underline{\underline{\varepsilon}} = \mathrm{diag}(\varepsilon_1, \varepsilon_2, \ldots, \varepsilon_{\mathrm{MO}})$, as follows

$$\begin{aligned}\underline{\underline{H}}_{\mathrm{sys}} &= \underline{\underline{U}}^{\dagger}_{\mathrm{sys}}\ \underline{\underline{\varepsilon}}\ \underline{\underline{U}}_{\mathrm{sys}} \\ &= \begin{pmatrix} \underline{\underline{H}}_{\mathrm{L}} & \underline{\underline{V}}_{\mathrm{LM}} & 0 \\ \underline{\underline{V}}^{\dagger}_{\mathrm{LM}} & \underline{\underline{H}}_{\mathrm{M}} & \underline{\underline{V}}_{\mathrm{MR}} \\ 0 & \underline{\underline{V}}^{\dagger}_{\mathrm{MR}} & \underline{\underline{H}}_{\mathrm{R}} \end{pmatrix}\end{aligned} \tag{S18}$$

The rectangular matrices $\underline{\underline{V}}_{\mathrm{LM}}$ and $\underline{\underline{V}}_{\mathrm{MR}}$ describe the couplings from the extended molecule to the respective lead, in the local pseudo-spectral basis. Note that the interlead coupling matrix $\underline{\underline{V}}_{\mathrm{LR}}$ is not strictly zero but vanishingly small. The total unitary transformation,

$\underline{\underline{U}}_{\mathrm{sys}}$, allows to numerically define an orthonormal set of pseudo-spectral one-electron basis functions from a subset of MOs obtained from standard quantum chemistry calculations. It takes a block diagonal form

$$\underline{\underline{U}}_{\mathrm{sys}} = \begin{pmatrix} \underline{\underline{U}}_{\mathrm{L}} & 0 & 0 \\ 0 & \underline{\underline{U}}_{\mathrm{M}} & 0 \\ 0 & 0 & \underline{\underline{U}}_{\mathrm{R}} \end{pmatrix} \tag{S19}$$

This yields three subsets of basis functions for the left lead $\left\{\left|\psi_a^{\mathrm{L}}\right\rangle\right\}_{n_{\mathrm{L}}}$, the right lead $\left\{\left|\psi_a^{\mathrm{R}}\right\rangle\right\}_{n_{\mathrm{R}}}$, and the extended molecule $\left\{\left|\psi_a^{\mathrm{M}}\right\rangle\right\}_{n_{\mathrm{M}}}$, which are then used in dynamical simulations and their analysis.

Parametrization of a Tight-Binding Model

Since the number of transport channels is limited by the number of available lead states, the resolution of the electronic current at a given bias voltage can be quite low. To circumvent this issue, we extend the leads by parameterizing a tight-binding Hamiltonian, $\underline{\underline{H}}_{\mathrm{tb}}$ from the elements of the lead dimer, Eq. (S13), similar to the procedure introduced in Ref. [S9]. The procedure is sketched in the bottom panel of Fig. S1. First, the lead diagonal blocks of the Hamiltonian Eq. (S18) are replaced by the dimer diagonal blocks, $\underline{\underline{H}}_{\mathrm{L/R}} \approx \underline{\underline{\tilde{H}}}_{\mathrm{L/R}}$. The off-diagonal blocks $\underline{\underline{\tilde{T}}}$ describing the coupling between two lead units in energy space are then used to add a new unit to the lead. This procedure can be repeated until convergence of the current through the nanojunction is obtained.

The new lead blocks are further divided into two groups: those belonging to a buffer region, $\underline{\underline{H}}^{\mathrm{buff}}_{\mathrm{L/R}}$, and lead units $\underline{\underline{H}}^{\mathrm{lead}}_{\mathrm{L/R}}$. Only the latter are coupled to the implicit electronic reservoir in order to enhance the resolution of the electronic current. The former are assigned to the extended molecule region and contribute significantly to the convergence of the DLvN towards NEGF reference calculations by avoiding direct coupling between the electronic reservoir and the scattering region. Note that, for all non-equilibrium Green's function (NEGF) reference calculations shown in this work, the tight-binding Hamiltonian serves

directly as input. This simplifies comparison of the currents obtained via the DLvN and NEGF formalisms.

For the propagation using the DLvN formalism, $\underline{\underline{H}}_{\mathrm{tb}}$ is brought into the form of $\underline{\underline{H}}_{\mathrm{sys}}$ (cf. Eq. (S18)) by diagonalization of the extended molecule, the left and right lead blocks. For clarity, we will refrain from introducing a new symbol for this final Hamiltonian here. Instead, we will refer to Eq. (S18) hereafter. Since all states are propagated explicitly in the DLvN equation, extension of the tight binding Hamiltonian greatly increases the associated computational effort. We observed that pruning the MO basis at this stage, as proposed in elsewhere,[S2] reduces the numerical effort at the expense of a violation of the Pauli principle.

Procedure to Monitor the Electron Dynamics

In the DLvN formalism, the time-evolution of the block of the density matrix corresponding to the extended molecule can be written by exploiting the structure of the localized Hamiltonian Eq. (S18) as follows

$$\begin{aligned}\frac{\partial \underline{\underline{\rho}}_{\mathrm{M}}(t)}{\partial t} = &-\frac{\imath}{\hbar}\left[\underline{\underline{H}}_{\mathrm{M}}, \underline{\underline{\rho}}_{\mathrm{M}}(t)\right] \\ &-\frac{\imath}{\hbar}\left(\underline{\underline{V}}_{\mathrm{ML}}\underline{\underline{\rho}}_{\mathrm{LM}}(t) - \underline{\underline{\rho}}_{\mathrm{ML}}(t)\underline{\underline{V}}_{\mathrm{LM}}\right) \\ &-\frac{\imath}{\hbar}\left(\underline{\underline{V}}_{\mathrm{MR}}\underline{\underline{\rho}}_{\mathrm{RM}}(t) - \underline{\underline{\rho}}_{\mathrm{MR}}(t)\underline{\underline{V}}_{\mathrm{RM}}\right),\end{aligned} \tag{S20}$$

Taking the trace, $\mathrm{Tr}\left\{\frac{\partial \underline{\underline{\rho}}_{\mathrm{M}}(t)}{\partial t}\right\}$, yields the temporal change of the total number of electrons in the extended molecule.[S2] This quantity comprises three contributions: i) the probability flux within the extended molecule, ii) the probability flux from the left lead to the central unit (the influx), and iii) the probability flux from the right lead to the central unit (the outflux). Under steady-state conditions, the probability flux within the extended molecule vanish, as well as the sum of the latter two contributions. Thus, the total number of electrons in the extended molecule stays unchanged. Multiplying the influx and the outflux by the

elementary charge e, yields the current per spin channel[S4]

$$\begin{aligned} I_{\mathrm{LM}}(t) = &\quad \frac{2e}{\hbar} \sum_{a}^{N_{\mathrm{L}}} \sum_{b}^{N_{\mathrm{M}}} \underline{\underline{V}}_{\mathrm{LM}}^{(a,b)} \, \mathrm{Im} \left\{ \underline{\underline{\rho}}_{\mathrm{LM}}^{(a,b)}(t) \right\} \\ I_{\mathrm{MR}}(t) = &- \frac{2e}{\hbar} \sum_{a}^{N_{\mathrm{R}}} \sum_{b}^{N_{\mathrm{M}}} \underline{\underline{V}}_{\mathrm{RM}}^{(a,b)} \, \mathrm{Im} \left\{ \underline{\underline{\rho}}_{\mathrm{RM}}^{(a,b)}(t) \right\}. \end{aligned} \tag{S21}$$

The average of these values describes the net current passing through the junction

$$I(t) = \left(I_{\mathrm{LM}}(t) + I_{\mathrm{MR}}(t) \right)/2, \tag{S22}$$

where for a steady state, the condition $I_{\mathrm{LM}}(t) = I_{\mathrm{MR}}(t)$ holds.

Alternatively, the local current in the scattering region can be extracted from the time-dependent density operator, which in the basis of the localized eigenstates takes the following form

$$\underline{\underline{\hat{\rho}}}\,(t) = \sum_{a,b}^{n_{\mathrm{MO}}} \underline{\underline{\rho}}^{\,(a,b)}(t) \left| \varphi_a \right\rangle \left\langle \varphi_b \right|. \tag{S23}$$

To compute the local current in the region of space localized on the extended molecule, it suffice to project the driven Liouville von-Neumann equation Eq. (S1) in position representation

$$\begin{aligned} \frac{\partial \left\langle \vec{r} \middle| \underline{\underline{\hat{\rho}}}\,(t) \middle| \vec{r} \right\rangle}{\partial t} &= -\frac{\imath}{\hbar} \left\langle \vec{r} \middle| \left[\hat{H}, \underline{\underline{\hat{\rho}}}\,(t) \right] \middle| \vec{r} \right\rangle - \frac{\imath}{\hbar} \left\langle \vec{r} \middle| \left[\imath \hat{W}, \underline{\underline{\hat{\rho}}}\,(t) \right]_{+} \middle| \vec{r} \right\rangle \\ &= -\frac{\imath}{\hbar} \left\langle \vec{r} \middle| \left[-\frac{\hbar^2}{2m_e} \nabla_e^2 + \hat{v}_{\mathrm{KS}}, \underline{\underline{\hat{\rho}}}\,(t) \right] \middle| \vec{r} \right\rangle + \mathcal{W}(\vec{r}, t), \end{aligned} \tag{S24}$$

Since the effective potential $\hat{v}_{\mathrm{KS}}$ is a multiplicative operator in position representation and the complex Hamiltonian $\imath \hat{W}$ acts only onto the lead basis functions, Eq. (S29) simplifies to the electronic continuity equation for the extended molecule volume

$$\frac{\partial \rho_{\mathrm{M}}(\vec{r}, t)}{\partial t} = -\vec{\nabla}_e \cdot \vec{j}_{\,\mathrm{M}}(\vec{r}, t), \tag{S25}$$

where the time derivative of the electron density is referred to as electronic flow. Note that,

since the lead eigenfunctions, $\left\{\psi_a^{\mathrm{L/R}}(\vec{r})\right\}_{n_{\mathrm{L/R}}}$ are negligibly small in the scattering region due to the localization procedure, the basis functions introduced by the tight-binding extension can also be safely ignored. Hence, the time-dependent electronic (probability) flux density at a given point localized in the scattering region is given by

$$\vec{j}_{\mathrm{M}}(\vec{r},t) = \sum_{a<b} 2\imath\,\mathrm{Im}\left\{\underline{\underline{\rho}}_{\mathrm{M}}^{(a,b)}\right\}\vec{j}_{\mathrm{M}}^{(a,b)}(\vec{r}) \tag{S26}$$

where the time-independent state-to-state electronic flux density is defined as

$$\vec{j}_{\mathrm{M}}^{(a,b)}(\vec{r},t) = -\frac{\imath\,\hbar}{2m_e}\left(\varphi_a^{\mathrm{M}}(\vec{r})\vec{\nabla}_e\varphi_b^{\mathrm{M}}(\vec{r}) - \varphi_b^{\mathrm{M}}(\vec{r})\vec{\nabla}_e\varphi_a^{\mathrm{M}}(\vec{r})\right). \tag{S27}$$

For consistency with the current definition $I(t)$, Eq. (S25) is multiplied with the elementary charge to obtain the continuity equation for charge conservation relating the electronic charge density, $e\cdot\rho_{\mathrm{M}}(\vec{r},t)$, with the electronic current density, $\vec{J}_{\mathrm{M}}(\vec{r},t) = e\cdot\vec{j}_{\mathrm{M}}(\vec{r},t)$. Interestingly, the negative integral over $\vec{J}_{\mathrm{M}}(\vec{r},t)$ corresponds to the electronic dipole moment in velocity gauge.[S10,S11]

Computational Details

All quantum chemical calculations were performed using the quantum chemistry program TURBOMOLE[S13] at the density functional theory (DFT) level of theory using the PBE0[S14] hybrid functional and a def2-SVP basis set.[S15] Three structures have been considered: the ON conformer ($\theta \approx 0°$, cf. Fig. S2) and the OFF conformer ($\theta \approx 90°$, cf. Fig. 1 of the main manuscript) of the molecular junction as depicted in Fig. S1 (upper panel), as well as the lead dimer, as depicted in Fig. S1 (central panel). The size of the lead sections in the extended molecule section is chosen large enough such that the influence of the central nitrophenyl group on the leads is negligible. Further, the mechanistic details of the spatially resolved current dynamics can be investigated on a larger part of the so-called "extended" molecule.

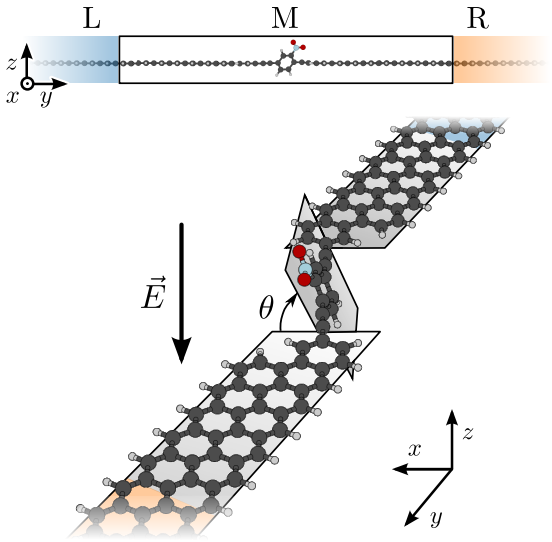

Figure S2: Cartoon of the investigated OPE-GNR nanojunction viewed from different perspectives. Carbon atoms are colored in dark grey, hydrogen atoms in light grey, nitrogen atoms in light blue, and oxygen atoms are colored in red. As demonstrated in Ref.[S12], an electric field along the z-axis, $\vec{E}$, can be used to switch the device from a conducting state (ON, $\theta \approx 0°$) to a less conducting state (OFF, $\theta \approx 90°$). For the investigation of the electron current dynamics, the device is divided into three segments: the left lead (L, highlighted in blue), the extended molecule (M, black solid box), and the right lead (R, highlighted in orange). The color code and the coordinate system defined in this figure are used throughout this work.

Note that, in previous work, the NEGF reference was shown to be already converged with smaller leads.[S12,S16]

The reference current-voltage characteristics ($I - V$ curve) of the molecular switching device was obtained from the tight-binding Hamiltonian depicted in Fig. S1 (lower panel) using the non-equilibrium Green's function method and the Landauer-Büttiker formalism, as implemented in the program ASE (Atomic Simulation Environment).[S17–S21] This implementation has also been used to obtain the lead's self-energy (cf. Eq. (S6)). The propagation of the reduced density matrix was performed at $T = 0\,\mathrm{K}$ using the program GLOCT (Guided Locally Optimal Control Theory),[S22] an in-house implementation of a Markovian master equation propagator based on a preconditioned adaptive step size Runge-Kutta algorithm.[S23] In the simulation, the time step size was found to vary between $\Delta t = 0.001\,\mathrm{as}$ and $\Delta t = 150\,\mathrm{as}$ with an average value of $\Delta t = 30\,\mathrm{as}$.

For the computation of the electron density and electronic current density, the molecular orbitals and the spatial derivatives thereof were first projected on a grid using the program ORBKIT.[S24] These quantities were combined with the time-dependent coefficients of the reduced density matrix with our open-source PYTHON package DETCI@ORBKIT.[S11,S25] The results were visualized using PYTHON package MATPLOTLIB.[S26] All streamline plots of the current density were created using the program suite AMIRA.[S27] Here, a few hundred streamlines are seeded in the volume surrounding the left lead region (blue box in Fig. S1 (upper panel)) for positive and the right lead region (orange box in Fig. S1 (upper panel)) for negative bias voltages according to the magnitude of the electron density in that volume. The color and opacity of the streamlines is chosen according the magnitude of the current density. The depictions of the molecular structures in Fig. 1 of the main manuscript and Fig. S1 were created using the program XCRYSDEN.[S28]

Convergence Behavior of the Method

Localization Procedure

The localization procedure depends on two energy parameters: ΔE_{lead} for choosing the lead basis functions and ΔE_{basis} for choosing the basis set of the complete system. To estimate the convergence of the localization procedure, Fig. S3 reports the influence of the energy windows on the transmission function within the energy range of interest. For the system investigated, we focus on the conductance around the Fermi energy within an energy window of $U_{\text{max}} = 4\,\text{V}$. The prominent feature around the Fermi level observed in the reference NEGF results can only be reproduced accurately using a very large basis ($\Delta E_{\text{lead}} = 40\,\text{eV},\ \Delta E_{\text{basis}} = 80\,\text{eV}$, black line). For the smallest possible energy windows ($\Delta E_{\text{lead}} = 4\,\text{eV},\ \Delta E_{\text{basis}} = 4\,\text{eV}$, dark blue line) qualitatively meaningful results are only obtained between $-2\,\text{eV}$ and $2\,\text{eV}$. Using a very large window for the resolution-of-identity, $\Delta E_{\text{basis}} = 80\,\text{eV}$, while keeping the number of lead states small ($\Delta E_{\text{lead}} = 4\,\text{eV}$, light blue line). does not improve the appearance of

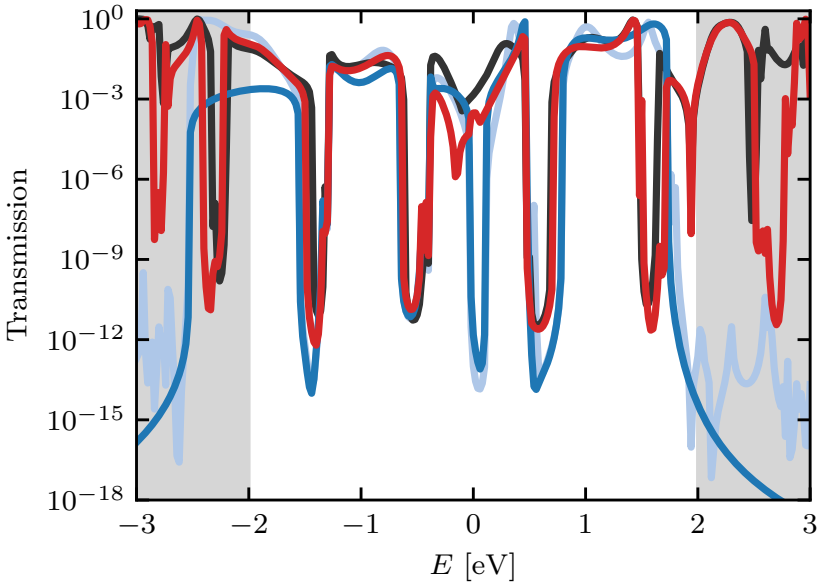

Figure S3: The transmission function within the energy range of interest (conductance around the Fermi energy within an energy window of $U_{\mathrm{max}} = 4\,\mathrm{V}$) for different choices of the two energy parameters used within the localization procedure: ΔE_{lead} for choosing the lead basis functions and $\Delta E_{\mathrm{basis}}$ for choosing the basis set of the complete system. Dark blue line: the minimum energy ranges ($\Delta E_{\mathrm{lead}} = 4\,\mathrm{eV}$, $\Delta E_{\mathrm{basis}} = 4\,\mathrm{eV}$), light blue line: the minimal choice for the size of the lead basis ($\Delta E_{\mathrm{lead}} = 4\,\mathrm{eV}$, $\Delta E_{\mathrm{basis}} = 80\,\mathrm{eV}$), red line: the energy range used in this work ($\Delta E_{\mathrm{lead}} = 6\,\mathrm{eV}$, $\Delta E_{\mathrm{basis}} = 8\,\mathrm{eV}$), and black line: a reference ($\Delta E_{\mathrm{lead}} = 40\,\mathrm{eV}$, $\Delta E_{\mathrm{basis}} = 80\,\mathrm{eV}$).

the conductance curve. On the contrary, a moderate increase of the lead energy window ($\Delta E_{\mathrm{lead}} = 6\,\mathrm{eV}$) and of the resolution-of-identity ($\Delta E_{\mathrm{basis}} = 8\,\mathrm{eV}$) allows to recover all features of the reference (see red line in Fig. S3) at a tractable numerical cost. These are the parameters used throughout this work, which gives rise to $n_{\mathrm{M}} = 52$ localized basis function in the scattering region and $n_{\mathrm{L/R}} = 9$ lead functions, without considering any tight-binding extension.

Tight-Binding Model

Using the coupling elements of the Hamiltonian matrix of the lead dimer $\underline{\underline{\tilde{T}}}$, the system Hamiltonian can be extended at will by adding additional buffer $\underline{\underline{\tilde{H}}}^{\mathrm{buff}}_{\mathrm{L/R}}$ and lead units $\underline{\underline{\tilde{H}}}^{\mathrm{lead}}_{\mathrm{L/R}}$,

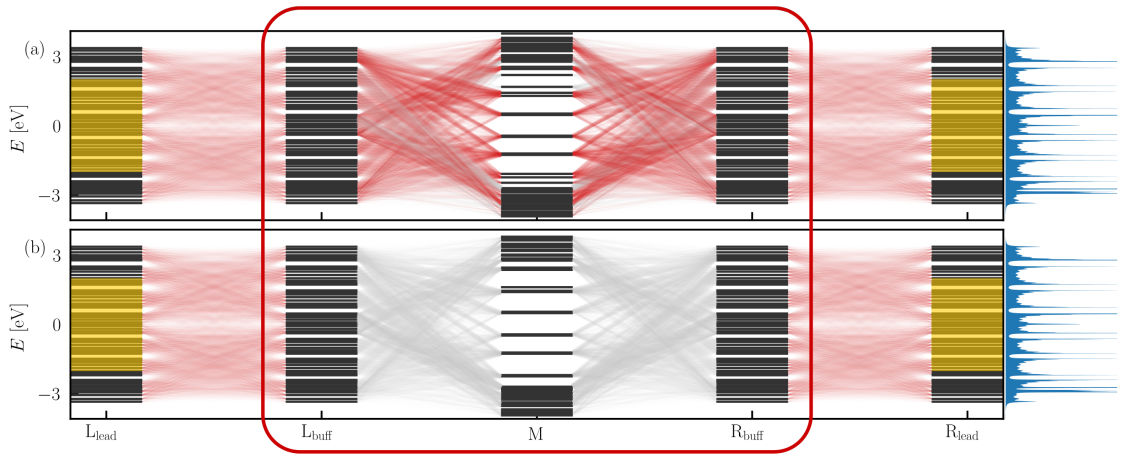

Figure S4: Energy levels (black horizontal lines) and their couplings (red and grey lines) for the ON (upper panel) and the OFF conformer (lower panel) extended with ten buffer and ten lead units showing the three parts of the junction: the left lead (L_{lead}), the extended molecule ($L_{buff} + M + R_{buff}$, red box), and the right lead (R_{lead}). The extended molecule (red box) consists of left and right buffer units L_{buff} and R_{buff} and the original extended molecule region (M, cf. black solid box in Fig. S1 (upper panel)). It is treated as the coherent scattering region in Eq. (S18). The linewidth of the connectors between states is chosen according to the coupling strength. To allow identifying the conducting states, the connectors are colored in red if the coupling of a specific state of the extended molecule with both, the left and the right buffer units, differs by at most a factor of 2 for the largest component on each lead. The density of states of the leads, depicted as blue shaded curve at the abscissa, is broadened with a Lorentzian of the same width as in the subsequent DLvN propagations (cf. Eq. (S6)). The yellow shaded areas highlight the maximum Fermi transport window of 4 V. The depiction of the diagonal elements of the Hamiltonian blocks as energy levels and their couplings as lines connecting these levels to visualize the structure of the Hamiltonian was already proposed in Ref.[S2,S5]

as proposed elsewhere[S9]. Fig. S4 shows the spectrum of the resulting Hamiltonian for the ON (upper panel) and OFF (lower panel) conformations for an exemplary system with ten buffer and ten lead units. The black horizontal lines refer to the energy levels of the different regions of the nanojunction, and the connectors between these energy levels correspond to the couplings between the pseudo-spectral states of the different regions, e.g., $\underline{\underline{V}}_{L_{buff}M/R_{buff}M}$. It can be observed that the energy spectrum of both logical states is nearly identical. While the spectrum of the extended molecule is dense at low and at high energies, the pseudo-eigenstates of both leads are more evenly distributed and form bands at intermediate energies, with an energy spacing between the bands of $\Delta\varepsilon \approx 0.2\,\mathrm{eV}$. At the ordinate, the density of

states (DOS) of the leads is plotted using the same Lorentzian broadening as defined by Eq. (S6).

The linewidth for interstate couplings in Fig. S4 is chosen according to the strength of the respective coupling. Interestingly, when we compare the ON and OFF conformations, not only the preferred coupling channels but also the coupling strengths are very similar. To distinguish between conductive and non-conductive channels through the bridge, we introduce a measure of the connectivity asymmetry of a particular molecular channels.[S5] That is, the connectors are only colored in red if the coupling to a specific molecular channel differs by a factor of 2 at most for the largest coupling on each lead. This reveals that the majority of the extended molecule states of the ON conformation are conductive, while for the OFF conformation, nearly all states are asymmetrically coupled to the leads and therefore non-conductive. The explanation can be found by analyzing the coupling to the (nearly) degenerate pairs of extended molecule states in more detail. For each pair of states localized on the extended molecule, the coupling strength is approximately the same with both leads in the ON conformation. For the OFF logical state, one state of the doublet couples exclusively to the left while the other couples exclusively to the right lead. Thus, it can be anticipated that the OFF conformation will be significantly less conducting than the ON logical state, even without performing any dynamical simulation.

Fig. S5 shows the time-evolution of the electronic current for both conformers at $T = 0\,\mathrm{K}$ subject to a linear voltage ramp from 0V (0ps) to 4V at 4ps, compared with the current voltage characteristics obtained from NEGF calculations at the same bias voltages (red curves). Regarding the NEGF reference, it can be noticed that the current gradually increases in smooth steps for the ON conformation (top and central panel of Fig. S5), while the current for the OFF logical state (bottom panel of Fig. S5) always remains very small. At all potential biases, the ON/OFF current ratio lies between 10^2 and 10^3, which is in good agreement with our previous findings.[S12] The finite number of states within the time-dependent DLvN simulation restricts the effective applicable bias voltages to the available lead state energies.

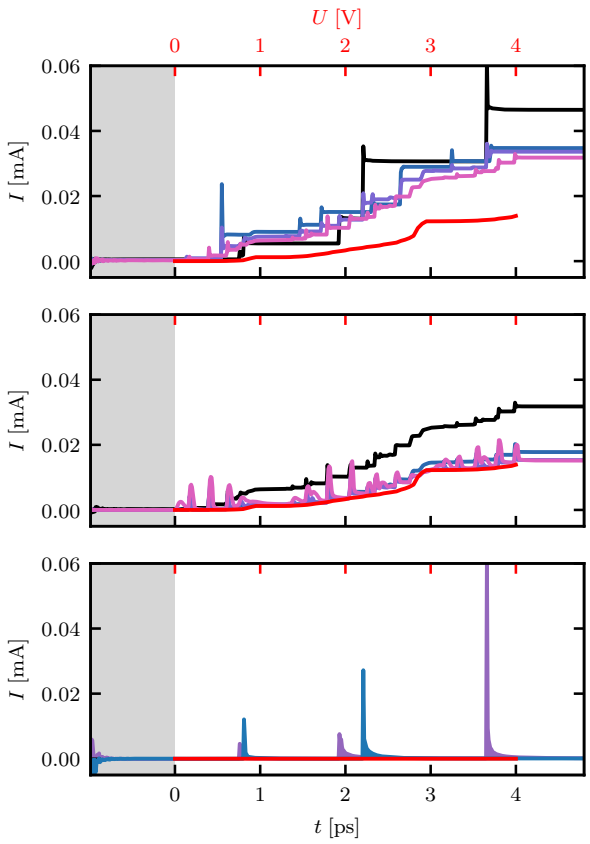

Figure S5: Time-dependent current-voltage characteristic ($I-V$ curve) of the OPE-GNR junction $I(t)$ applying a linear voltage ramp from $U(t=0\,\mathrm{ps})=0$ to $U(t=4\,\mathrm{ps})=4\,\mathrm{V}$ for ON (upper and central panel), and for OFF (lower panel) compared with NEGF reference calculations (red lines). The grey shaded area highlights the equilibration time without bias voltage to account for the unphysical behavior at the beginning of the dynamics. Upper panel: The time-dependent current for the original system (cf. Fig. S1 upper panel), and for two, five, and ten lead units (color key: black, dark blue, purple, and pink, respectively). Central panel: The time-dependent current for ten lead units with zero (black), one (dark blue), two (purple) and ten (pink) buffer units. Lower panel: The two components contributing to the net current $I(t)$, i.e., the influx from the left lead ($I_{\mathrm{LM}}(t)$) and the negative outflux to the right lead ($-I_{\mathrm{MR}}(t)$), are plotted as blue and purple curves for the OFF conformer without tight-binding extension.

For example, only four steps can be observed within the time-dependent current dynamics for the ON conformation (black curve in the upper panel of Fig. S5). The NEGF reference and the time-dependent results share the same qualitative features despite some marked deviations. That is, both curves describe the same few transport channels showing up at the same bias voltages.

Whenever the time-dependent bias voltage hits a resonance in a lead state, a rapid rise in conductivity is observed followed by an equilibration to a lower lying plateau. This rapid rise is observed for both the ON and OFF logical states. To understand this phenomenon, the two contributions to the current, $I(t)$, (cf. Eq. (S22)) are plotted separately in the lower panel of Fig. S5 for the OFF configuration: the influx from the left lead ($I_{\mathrm{LM}}(t)$) as a blue and the negative outflux to the right lead ($-I_{\mathrm{MR}}(t)$) as a purple curve. As can be seen from the figure, there is either an influx or an outflux in this OFF configuration, but never both simultaneously. These dynamical features, which take place in the femtosecond time regime, can be associated with the population and depopulation of extended molecular states reacting to the new boundary conditions. Thus, those peak currents do not contribute to the overall current passing *through* this junction, and should be understood as an ultrafast equilibration response.

In order to enable a more precise description of the electric current dynamics for the ON state, both leads were extended as explained above (see Eq. S15) by a certain number of tight binding units as buffer units between the central molecule and the leads and as additional lead units being coupled to the implicit electronic reservoir. While the latter allow for a higher resolution in the bias voltages and a better representation of the density of states in the leads, the former prevents the direct coupling between the central unit and the implicit electron reservoir.[S5] For the ON conformation, the results for two (dark blue), five (purple), and ten (pink) lead units are shown in the upper panel of Fig. S5. It can be recognized that, with increasing number of lead units, the large jumps in $I(t)$ between the different plateaus are gradually replaced by smoother transitions, and the curves converge slowly to reproduce the shape of the NEGF reference. Moreover, the size of the peak currents due to the ultrafast equilibration dynamics is significantly reduced due to the smaller energy gap between the states. Interestingly, simulations at higher temperatures without tight-binding extension yield similar $I-V$ current profiles. This is due to the smoother change in population as temperature increases, see Eq. (S2).

The central panel of Fig. S5 shows the influence of introducing buffer units, i.e., lead units that are not coupled to the electronic reservoir, at the example of ten lead units with zero (black), one (dark blue), two (purple) and ten (pink) buffer units. As can be seen, introducing just a single buffer unit (dark blue curve) significantly improves the result, and by adding two or more buffer units the $I-V$ curve is basically converged to the NEGF reference (red curve). Interestingly, the more buffer units we introduce, the more pronounced are the features occurring when a new transport channel is opened. This phenomenon can be explained by the simple fact that increasing the number of states in the buffer implies more phases needing to equilibrate. This is a signature of memory effects during the equilibration dynamics, an important feature of the DLvN formalism.

Time Evolution of the Pseudo-Spectral State Populations

To confirm that the Pauli principle is satisfied by the density matrix obtained from the driven Liouville-von Neumann simulations, we can monitor the population of the pseudo-spectral states used in the basis. As a rule of thumb, the Pauli principle can be said to be satisfied provided all populations always lie between zero and one at all times. It was shown that the DLvN equation, as an approximation to the NEGF formalism,[S1] is formally Markovian and ensures semi-positivity of the one-electron reduced density matrix.[S3,S29] As can be seen from Fig. S6, this condition is indeed respected throughout our simulation, also at large biases. As the bias voltage increases, new transport channels are subsequently populated and depopulated. The subsequent relaxation dynamics towards population equilibration can take up to picoseconds. In the right panel, more channels are present due to the tight-binding extension but the general behaviour remains the same and the Pauli principle remains fulfilled.

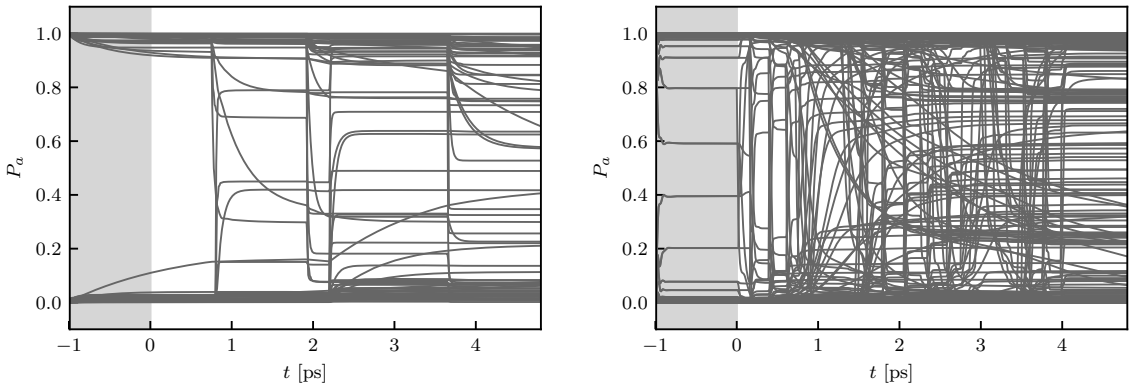

Figure S6: Time-dependent state populations of the OPE-GNR junction under a linear voltage ramp from $U(t = 0\,\mathrm{ps}) = 0$ to $U(t = 4\,\mathrm{ps}) = 4\,\mathrm{V}$ for the ON conformation (cf. Fig. 5). Left panel: The time-dependent populations for the system without tight-binding extension. Right panel: The time-dependent populations for a system extended using the tight-binding Hamiltonian with ten buffer and ten lead units.

Convergence of the Electronic Continuity Equation

In this section, we present two perspectives to estimate the convergence of the electronic continuity equation in position space: from the time-evolution of the block of the density matrix corresponding to the extended molecule (cf. Eq. 18) in position representation

$$\frac{\partial \left\langle \vec{r} \middle| \underline{\underline{\rho}}_{\mathrm{M}}(t) \middle| \vec{r} \right\rangle}{\partial t} = \underbrace{-\frac{\imath}{\hbar} \left\langle \vec{r} \middle| \left[\underline{\underline{H}}_{\mathrm{M}}, \underline{\underline{\rho}}_{\mathrm{M}}(t) \right] \middle| \vec{r} \right\rangle}_{+\widetilde{\varrho}_{\mathrm{M}}(\vec{r},t)} \underbrace{-\frac{\imath}{\hbar} \left\langle \vec{r} \middle| \left(\underline{\underline{V}}_{\mathrm{ML}} \underline{\underline{\rho}}_{\mathrm{LM}}(t) - \underline{\underline{\rho}}_{\mathrm{ML}}(t) \underline{\underline{V}}_{\mathrm{LM}} \right) \middle| \vec{r} \right\rangle}_{+\widetilde{\varrho}_{\mathrm{LM}}(\vec{r},t)} \underbrace{-\frac{\imath}{\hbar} \left\langle \vec{r} \middle| \left(\underline{\underline{V}}_{\mathrm{MR}} \underline{\underline{\rho}}_{\mathrm{RM}}(t) - \underline{\underline{\rho}}_{\mathrm{MR}}(t) \underline{\underline{V}}_{\mathrm{RM}} \right) \middle| \vec{r} \right\rangle}_{+\widetilde{\varrho}_{\mathrm{RM}}(\vec{r},t)} , \tag{S28}$$

or from the position representation of the full driven Liouville-von Neumann equation

$$\frac{\partial \left\langle \vec{r} \middle| \underline{\underline{\hat{\rho}}}(t) \middle| \vec{r} \right\rangle}{\partial t} = \underbrace{-\frac{\imath}{\hbar} \left\langle \vec{r} \middle| \left[\hat{H}, \underline{\underline{\hat{\rho}}}(t) \right] \middle| \vec{r} \right\rangle}_{-\vec{\nabla}_e \cdot \vec{j}_{\mathrm{M}}(\vec{r},t)} \underbrace{-\frac{\imath}{\hbar} \left\langle \vec{r} \middle| \left[\imath \hat{W}, \underline{\underline{\hat{\rho}}}(t) \right]_+ \middle| \vec{r} \right\rangle}_{\mathcal{W}(\vec{r},t)} . \tag{S29}$$

The right hand sides of both equations each consist of two parts: the coherent (blue terms) and the driving part (green terms). In Eq. (S28), the electron flow within the extended molecule $\widetilde{\varrho}_{\mathrm{M}}(\vec{r},t)$ describes the coherent electronic contribution, and the incoherent flow of electrons from the leads to the central unit is given by $\widetilde{\varrho}_{\mathrm{LM}}(\vec{r},t) + \widetilde{\varrho}_{\mathrm{RM}}(\vec{r},t)$. In Eq. (S29), the spatial divergence of the flux density $-\vec{\nabla}_e \cdot \vec{j}_{\mathrm{M}}(\vec{r},t)$ is used to describe the coherent electron flow, and the complex Hamiltonian $\mathcal{W}(\vec{r},t)$ yields the incoherent contribution to the electronic current, which we dub "driving term".

Integrating the above quantities over a volume Ω_y with proper boundary conditions,

$$\begin{array}{lll} x_{\min} = -\infty & y_{\min} = -\infty & z_{\min} = -\infty \\ x_{\max} = +\infty & y_{\max} = y & z_{\max} = +\infty \end{array} . \tag{S30}$$

and multiplying the results by the elementary charge, yields relations for the charge conservation along the transport axis for each value of $y \in \mathrm{M}$ on the extended molecule. For a quasi-stationary state, the coherent and the driving term have opposite signs and should have the same absolute value, i.e.,

$$\begin{aligned} I(t) &= e \iiint_{\Omega_y} \widetilde{\varrho}_{\mathrm{M}}(\vec{r},t)\mathrm{d}^3\Omega_y && = -e \iiint_{\Omega_y} \Big(\widetilde{\varrho}_{\mathrm{LM}}(\vec{r},t) + \widetilde{\varrho}_{\mathrm{RM}}(\vec{r},t)\Big)\mathrm{d}^3\Omega_y \\ &= e \iiint_{\Omega_y} \Big(-\vec{\nabla}_e \cdot \vec{j}_{\,\mathrm{M}}(\vec{r},t)\Big)\,\mathrm{d}^3\Omega_y && = -e \iiint_{\Omega_y} \mathcal{W}(\vec{r},t)\mathrm{d}^3\Omega_y \\ &= e \oiint_{S_y} \Big(-\vec{j}_{\,\mathrm{M}}(\vec{r},t)\cdot\vec{n}_y\Big)\,\mathrm{d}^2S(y). \end{aligned} \tag{S31}$$

The last line is a consequence of the divergence theorem for vanishing current far away from the molecular device in the direction perpendicular to the electron flow. The Eqs. (S31) can be used to evaluate the convergence of continuity equation with respect to the basis set, the grid, and the method in general.

Fig. S7 shows these contributions for a representative snapshot for $U = 4.0\,\mathrm{V}$ at $t = 4.8\,\mathrm{ps}$ in the ON conformation. All contributions have the same general behavior: the absolute value rises until the boundaries of the central molecule ($y \approx -20\,\mathrm{Å}$) to a plateau with the height of $I(t)$ (black dashed dotted line, cf. Eq. (S22)). The value stays constant within the spatial extent of the extended molecule, until it finally decreases again for $y \gtrsim 20\,\mathrm{Å}$. The deviations from the $I(t)$ reference computed using Eq. (S22) are smaller for the contributions derived from the density than those derived from the flux density (blue and orange curve in the right panel of Fig. S7). In particular, $e \iiint_{\Omega_y}\Big(-\vec{\nabla}_e \cdot \vec{j}_{\,\mathrm{M}}(\vec{r},t)\Big)\,\mathrm{d}^3\Omega_y$ shows small oscillations, which can be attributed to the inaccurate representation of the cusps on the atoms

when using atom-centered Gaussian functions as a primitive basis set. This limitation was described in detail in Ref.[S11]

The simulation has been performed without any tight-binding extension at the PBE/def2-SVP level of theory. Energy windows of $\Delta E_{\text{lead}} = 6\,\text{eV}$, $\Delta E_{\text{basis}} = 8\,\text{eV}$ were used for the localization. Note that tight-binding extensions within this work are done in the energy space, and, consequently, no spatial information is available on the leads nor in the buffer region.

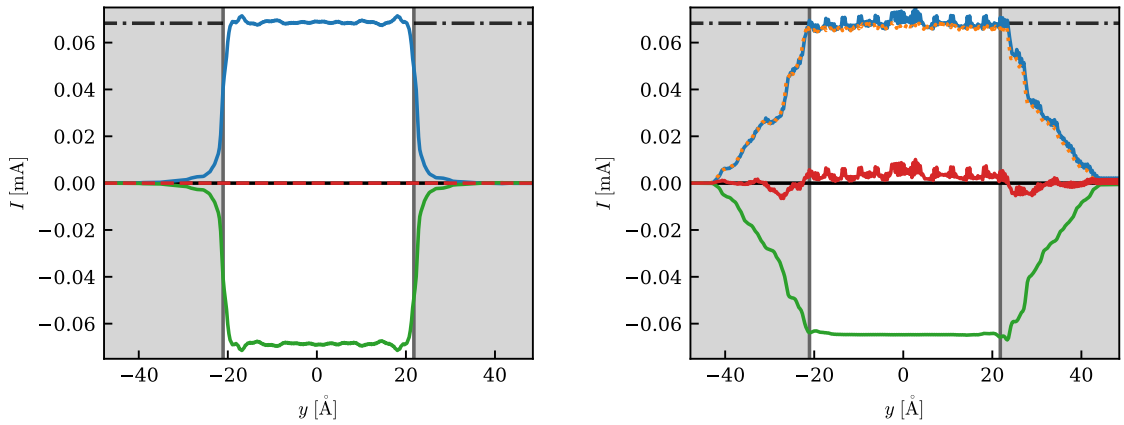

Figure S7: The quantities defined in Eq. (S31) exemplary shown for a representative snapshot at $t = 4.8\,\text{ps}$ for a simulation with a linear voltage ramp from $U(t = 0\,\text{ps}) = 0$ to $U(t = 4\,\text{ps}) = 4\,\text{V}$ for the ON conformation. The simulation has been performed without any tight-binding extension at the PBE/def2-SVP level of theory. Energy windows of $\Delta E_{\text{lead}} = 6\,\text{eV}$, $\Delta E_{\text{basis}} = 8\,\text{eV}$ were used for the localization. The black dashed dotted line is the reference value corresponding to the current definition as given in Eq. (S22). The black solid line corresponds to the integral over $\frac{\partial}{\partial t}\left\langle \vec{r}\middle|\underline{\underline{\hat{\rho}}}(t)\middle|\vec{r}\right\rangle$. Left panel: Quantities derived from Eq. (S28). Blue curve: the current within the extended molecule $e\iiint_{\Omega_y}\widetilde{\varrho}_{\text{M}}(\vec{r},t)\mathrm{d}^3\Omega_y$, and green curve: the current from the leads to the central unit $e\iiint_{\Omega_y}\big(\widetilde{\varrho}_{\text{LM}}(\vec{r},t)+\widetilde{\varrho}_{\text{RM}}(\vec{r},t)\big)\mathrm{d}^3\Omega_y$. The red dashed curve corresponds to the sum of both. Right panel: Quantities derived from Eq. (S29). Blue solid curve: the integral over the negative spatial divergence of the current density $e\iiint_{\Omega_y}\big(-\vec{\nabla}_e\cdot\vec{j}_{\text{M}}(\vec{r},t)\big)\mathrm{d}^3\Omega_y$, orange dotted curve: the surface integral over the current density $e\oiint_{S_y}\Big(-\vec{j}_{\text{M}}(\vec{r},t)\cdot\vec{n}_y\Big)\,\mathrm{d}^2S(y)$ and green curve: the integral over the position representation of the complex Hamiltonian $e\iiint_{\Omega_y}\mathcal{W}(\vec{r},t)\mathrm{d}^3\Omega_y$. The red curve corresponds to the sums of the blue and the green curves.

Cartesian coordinates of the molecules used to create the model Hamiltonian

Table S1: xyz coordinates for the ON conformation (in Å)

C	4.7595039	-14.2543448	-0.0003832
C	5.4262384	-13.0229127	-0.0033748
C	4.7323833	-11.8001763	-0.0029961
C	5.3974413	-10.5642221	-0.0051472
C	4.7042618	-9.3466562	-0.0038731
C	5.3816837	-8.1107031	-0.0035170
C	4.6986857	-6.8996228	-0.0009807
C	5.4038848	-5.6523052	0.0019494
C	2.6209020	-15.4981426	0.0056444
C	3.3122870	-14.2686499	0.0033304
C	2.5953274	-13.0445250	0.0037058
C	3.2854162	-11.8117984	0.0002994
C	2.5686391	-10.5881375	0.0002027
C	3.2577053	-9.3482965	-0.0018976
C	2.5404373	-8.1212997	-0.0014023
C	3.2544278	-6.8834082	-0.0005907
C	2.6044886	-5.6275883	0.0015809
C	1.1745745	-15.5129299	0.0093399
C	0.4820535	-14.2855249	0.0111987
C	1.1510125	-13.0625342	0.0075572
C	0.4584392	-11.8248613	0.0068627
C	1.1278210	-10.6139901	0.0028867
C	0.4336570	-9.3594888	0.0013893
C	1.1053737	-8.1776510	-0.0007575
H	0.5320753	-7.2506629	-0.0017496
H	1.5165450	-5.5653956	0.0013211
H	-0.6111743	-14.2955652	0.0143268
H	-0.6348647	-11.8329386	0.0093490
H	-0.6591238	-9.3687244	0.0020865
H	6.5193207	-13.0106673	-0.0059818
H	6.4905057	-10.5502961	-0.0072650
H	6.4748964	-8.1074966	-0.0043634
H	6.4965740	-5.6771164	0.0021300
C	-3.5115695	14.9499603	-0.0167634
C	-4.1759203	13.7174276	-0.0247036
C	-3.4794813	12.4959217	-0.0309258
C	-4.1420099	11.2590331	-0.0374217
C	-3.4460686	10.0426920	-0.0406751
C	-4.1208118	8.8059547	-0.0446601
C	-3.4352653	7.5959598	-0.0437693
C	-4.1387196	6.3483765	-0.0445521
C	-1.3759952	16.1979455	-0.0077940
C	-2.0642359	14.9668719	-0.0161153
C	-1.3447278	13.7441292	-0.0229440
C	-2.0324674	12.5099888	-0.0297207
C	-1.3132463	11.2876582	-0.0344701

C	-1.9997643	10.0464205	-0.0388144
C	-1.2807105	8.8200856	-0.0402774
C	-1.9915595	7.5811066	-0.0404683
C	-1.3404144	6.3241092	-0.0355560
C	0.0704978	16.2161934	-0.0069520
C	0.7660060	14.9894280	-0.0152315
C	0.0995673	13.7653787	-0.0223032
C	0.7945909	12.5290654	-0.0283648
C	0.1275654	11.3172864	-0.0337020
C	0.8240789	10.0640105	-0.0381031
C	0.1542579	8.8813814	-0.0407745
H	0.7297260	7.9557507	-0.0439614
H	-0.2522686	6.2720013	-0.0311509
H	1.8591396	15.0017018	-0.0148886
H	1.8878645	12.5396139	-0.0280292
H	1.9168838	10.0762325	-0.0388368
H	-5.2690860	13.7025475	-0.0254032
H	-5.2350846	11.2423696	-0.0388175
H	-5.2140501	8.8002588	-0.0469090
H	-5.2314365	6.3708233	-0.0481769
C	-2.0437895	5.1287280	-0.0341069
C	-3.4783411	5.1569956	-0.0397655
H	-4.0248194	4.2122782	-0.0395157
C	-1.3612077	3.8847485	-0.0258321
C	-0.7918072	2.8047306	-0.0175798
H	-1.9673718	0.3740612	-0.0116420
C	-0.8785089	0.3559725	-0.0075724
C	-0.1367600	1.5458890	-0.0090279
C	1.2716778	1.4478243	-0.0023340
C	1.8952231	0.2154067	0.0037225
C	1.1671573	-0.9977742	0.0034764
C	-0.2430164	-0.8773523	-0.0013527
N	-1.1154046	-2.0615170	-0.0004974
O	-0.5923038	-3.1523221	0.0025504
C	1.8888991	-2.2133126	0.0063303
H	2.9846995	0.1551483	0.0082599
C	2.5979112	-3.2080330	0.0061788
C	3.3109948	-4.4317846	0.0044902
H	5.2927430	-3.5159451	0.0077894
C	4.7447114	-4.4599147	0.0050366
O	-2.3128671	-1.8706796	-0.0028083
H	1.8694944	2.3611153	-0.0024512
C	4.8014355	-19.1703627	0.0006928
C	5.4723360	-17.9392769	-0.0003208
C	4.7830330	-16.7129999	0.0008658
C	5.4507376	-15.4797674	-0.0010885
C	3.3518090	-19.1822795	0.0029446
C	2.6404938	-17.9528382	0.0048066
C	3.3335453	-16.7263063	0.0039240
C	0.5200783	-19.1941964	0.0071661
C	1.1925059	-17.9650724	0.0074082
C	0.5023296	-16.7396264	0.0100727
H	-0.5730589	-19.2017940	0.0086717
H	-0.5908745	-16.7480319	0.0123272

H	6.5655023	-17.9316083	-0.0022833
H	6.5437800	-15.4687236	-0.0036329
C	4.8361806	-24.0839078	0.0005366
C	2.6937315	-25.3197644	0.0040487
C	3.3866917	-24.0941869	0.0023711
C	1.2442115	-25.3305085	0.0057840
C	0.5548405	-24.1051147	0.0055554
H	-0.5383721	-24.1133094	0.0066837
C	5.5075902	-22.8535548	-0.0007123
C	4.8186588	-21.6274213	0.0001898
C	5.4899123	-20.3969640	-0.0005386
C	2.6757813	-22.8638450	0.0028337
C	3.3690846	-21.6382360	0.0020418
C	2.6584057	-20.4080432	0.0033442
C	1.2263540	-22.8745706	0.0044559
C	0.5372649	-21.6493671	0.0053766
C	1.2094121	-20.4191606	0.0052102
H	-0.5559534	-21.6569982	0.0066935
H	6.6007518	-22.8459433	-0.0021803
H	6.5829736	-20.3899688	-0.0020316
C	-3.5701217	19.8635715	0.0118306
C	-4.2363475	18.6303957	0.0066247
C	-3.5422829	17.4070400	-0.0004105
C	-4.2067488	16.1726908	-0.0084286
C	-2.1205610	19.8801020	0.0123714
C	-1.4043856	18.6530920	0.0072317
C	-2.0928023	17.4241558	-0.0001658
C	0.7109195	19.9017046	0.0155048
C	0.0436472	18.6696166	0.0087796
C	0.7378225	17.4457930	0.0022198
H	1.8040483	19.9136241	0.0171859
H	1.8309665	17.4577255	0.0037491
H	-5.3294672	18.6181161	0.0068636
H	-5.2997929	16.1586910	-0.0082642
C	-3.6241227	24.7763249	0.0199267
C	-1.4864553	26.0198871	0.0220283
C	-2.1747466	24.7917534	0.0210910
C	-0.0370030	26.0358675	0.0234843
C	0.6568865	24.8129758	0.0240022
H	1.7499921	24.8255073	0.0254447
C	-4.2906830	23.5434202	0.0190481
C	-3.5970953	22.3200037	0.0180359
C	-4.2636813	21.0872098	0.0153768
C	-1.4591932	23.5640171	0.0210112
C	-2.1476144	22.3359141	0.0189337
C	-1.4320330	21.1083594	0.0168830
C	-0.0098819	23.5799210	0.0224692
C	0.6838913	22.3572988	0.0217312
C	0.0169076	21.1243229	0.0184490
H	1.7769749	22.3694176	0.0226880
H	-5.3837606	23.5313963	0.0185965
H	-5.3567254	21.0752778	0.0147670
C	4.8906684	-31.4506497	0.0075832
C	5.5617557	-30.2225073	0.0053247

C	4.8724269	-28.9955944	0.0050180
C	5.5435073	-27.7657214	0.0025494
C	4.8541774	-26.5400030	0.0022979
C	5.5252841	-25.3096582	0.0003253
C	2.7496929	-32.6862824	0.0120669
C	3.4430666	-31.4602357	0.0099959
C	2.7308456	-30.2309189	0.0099026
C	3.4238171	-29.0053169	0.0072883
C	2.7120461	-27.7754071	0.0067616
C	3.4050135	-26.5499951	0.0043317
C	1.3003133	-32.6975918	0.0146420
C	0.6103943	-31.4723418	0.0148843
C	1.2812806	-30.2420169	0.0122711
C	0.5916166	-29.0165379	0.0115969
C	1.2624571	-27.7862701	0.0088086
C	0.5728451	-26.5607799	0.0080184
H	-0.4827328	-31.4811047	0.0167611
H	-0.5014909	-29.0251856	0.0132171
H	-0.5203487	-26.5685212	0.0094640
H	6.6549228	-30.2140105	0.0035728
H	6.6365906	-27.7572396	0.0008507
H	6.6183682	-25.3012874	-0.0011233
C	4.9260800	-36.3576124	0.0087482
C	5.5974023	-35.1411290	0.0079071
C	4.9084844	-33.9048214	0.0088752
C	5.5797444	-32.6808167	0.0073149
C	3.4812754	-36.3682271	0.0108453
C	2.7683634	-35.1414610	0.0123922
C	3.4623432	-33.9144826	0.0112784
C	0.6495480	-36.3855571	0.0150819
C	1.3199242	-35.1527653	0.0147947
C	0.6295455	-33.9284374	0.0162636
H	-0.4435766	-36.3955039	0.0167098
H	-0.4635850	-33.9374112	0.0182532
H	6.6906548	-35.1333789	0.0061635
H	6.6729507	-32.6725572	0.0055103
H	5.5040455	-42.1987914	0.0042150
C	4.9618250	-41.2496182	0.0054795
H	3.3595835	-43.4298058	0.0038352
C	2.8114277	-42.4841726	0.0054803
C	3.5199593	-41.2897837	0.0064961
H	0.8697119	-43.4469811	0.0054479
C	1.4001753	-42.4919008	0.0064574
C	0.6910006	-41.3147130	0.0086690
H	-0.4018819	-41.3239356	0.0094565
C	5.6372036	-40.0740731	0.0059936
C	4.9451609	-38.8089412	0.0075494
C	5.6149807	-37.6044844	0.0074111
C	2.8030769	-40.0480613	0.0085538
C	3.4995362	-38.8238246	0.0091134
C	2.7865363	-37.5958927	0.0110200
C	1.3636797	-40.0578215	0.0098787
C	0.6707537	-38.8453657	0.0122177
C	1.3410814	-37.6067989	0.0129004

H	-0.4225572	-38.8556262	0.0133866
H	6.7301945	-40.0633037	0.0051472
H	6.7084232	-37.5966900	0.0060593
C	-3.7056203	32.1436990	0.0296001
C	-4.3722035	30.9130352	0.0248286
C	-3.6785460	29.6884010	0.0228843
C	-4.3450569	28.4559643	0.0208015
C	-3.6512969	27.2325257	0.0204970
C	-4.3178108	25.9995760	0.0195134
C	-1.5692616	33.3872159	0.0368182
C	-2.2580914	32.1585256	0.0309107
C	-1.5415319	30.9315367	0.0274667
C	-2.2300016	29.7033527	0.0241693
C	-1.5138675	28.4757522	0.0232311
C	-2.2021833	27.2476882	0.0217461
C	-0.1198657	33.4038302	0.0375330
C	0.5743863	32.1808014	0.0328652
C	-0.0919809	30.9479163	0.0287761
C	0.6020805	29.7247085	0.0269612
C	-0.0643354	28.4918920	0.0246889
C	0.6296612	27.2687493	0.0244637
H	1.6674929	32.1932130	0.0336507
H	1.6951617	29.7371203	0.0282917
H	1.7227554	27.2809257	0.0253247
H	-5.4653011	30.9007831	0.0238346
H	-5.4381436	28.4435960	0.0201283
H	-5.4108750	25.9874454	0.0183426
C	-3.7590742	37.0509613	0.0582123
C	-4.4257844	35.8319252	0.0501551
C	-3.7324164	34.5980139	0.0423705
C	-4.3991465	33.3714619	0.0346656
C	-2.3142922	37.0670091	0.0582799
C	-1.5968664	35.8426897	0.0507639
C	-2.2862825	34.6130170	0.0431429
C	0.5172538	37.0949200	0.0586080
C	-0.1484182	35.8594131	0.0510338
C	0.5463412	34.6373314	0.0439499
H	1.6103606	37.1086152	0.0588313
H	1.6394697	34.6500340	0.0441178
H	-5.5190402	35.8201606	0.0500007
H	-5.4923145	33.3593622	0.0335770
H	-4.3595480	42.8900767	0.0889711
C	-3.8138053	41.9428980	0.0844275
H	-2.2203480	44.1295637	0.0935080
C	-1.6684138	43.1860209	0.0893150
C	-2.3720733	41.9887162	0.0842016
H	0.2693663	44.1569020	0.0931171
C	-0.2572339	43.1994965	0.0891097
C	0.4566755	42.0250448	0.0839251
H	1.5494771	42.0394396	0.0838366
C	-4.4845494	40.7648046	0.0791322
C	-3.7874818	39.5023214	0.0725459
C	-4.4526090	38.2953282	0.0660228
C	-1.6502740	40.7497457	0.0783432

C	-2.3419409	39.5227513	0.0723265
C	-1.6242375	38.2973972	0.0655695
C	-0.2108963	40.7651786	0.0782850
C	0.4865738	39.5551778	0.0723944
C	-0.1788325	38.3138098	0.0656774
H	1.5798126	39.5696710	0.0725522
H	-5.5775143	40.7499102	0.0794028
H	-5.5460239	38.2836285	0.0663428

Table S2: xyz coordinates for the OFF conformation (in Å)

C	4.7555839	-14.2571258	-0.0020994
C	5.4187356	-13.0260950	-0.0085692
C	4.7186944	-11.8072252	0.0037012
C	5.3796245	-10.5722725	0.0075289
C	4.6800006	-9.3586904	0.0346716
C	5.3541517	-8.1245655	0.0489558
C	4.6657338	-6.9168674	0.0881918
C	5.3679650	-5.6709310	0.1142018
C	2.6188378	-15.5045207	0.0065629
C	3.3083386	-14.2736101	0.0060602
C	2.5855861	-13.0545411	0.0165709
C	3.2717973	-11.8221751	0.0197504
C	2.5490238	-10.6037420	0.0432052
C	3.2341205	-9.3644016	0.0544228
C	2.5126642	-8.1413364	0.0892860
C	3.2234553	-6.9061169	0.1103541
C	2.5686578	-5.6518603	0.1595130
C	1.1724327	-15.5218436	0.0131589
C	0.4754843	-14.2968467	0.0242444
C	1.1414288	-13.0757263	0.0294598
C	0.4425962	-11.8438021	0.0513440
C	1.1081831	-10.6335174	0.0611121
C	0.4086416	-9.3832707	0.0918581
C	1.0772856	-8.2012193	0.1064298
H	0.5013449	-7.2765416	0.1330274
H	1.4807117	-5.6031286	0.1831456
H	-0.6173321	-14.3148758	0.0322532
H	-0.6504084	-11.8597740	0.0646422
H	-0.6839614	-9.3996038	0.1064813
H	6.5117584	-13.0101804	-0.0192872
H	6.4725091	-10.5544187	-0.0052714
H	6.4471666	-8.1186646	0.0346267
H	6.4604103	-5.6931189	0.0970484
C	-3.5109894	14.9498385	-0.0159595
C	-4.1734488	13.7167441	-0.0182775
C	-3.4744943	12.4957496	-0.0199084
C	-4.1334764	11.2579770	-0.0148948
C	-3.4333942	10.0427472	-0.0104336
C	-4.1036840	8.8049641	-0.0003559
C	-3.4125156	7.5969073	0.0116521
C	-4.1099361	6.3472049	0.0277083
C	-1.3765295	16.2000258	-0.0124502

C	-2.0636060	14.9682262	-0.0183733
C	-1.3419884	13.7474158	-0.0252981
C	-2.0273392	12.5126442	-0.0241266
C	-1.3043459	11.2930124	-0.0231596
C	-1.9871632	10.0507552	-0.0139850
C	-1.2633129	8.8274056	-0.0052293
C	-1.9699585	7.5884379	0.0118022
C	-1.3118676	6.3336405	0.0347695
C	0.0699038	16.2195682	-0.0150057
C	0.7674698	14.9940272	-0.0264541
C	0.1021607	13.7706874	-0.0304492
C	0.8006919	12.5373270	-0.0345009
C	0.1365101	11.3252597	-0.0282123
C	0.8378434	10.0750269	-0.0235693
C	0.1719027	8.8910855	-0.0116243
H	0.7499134	7.9671668	-0.0068289
H	-0.2235199	6.2869443	0.0416968
H	1.8604265	15.0101403	-0.0315464
H	1.8938005	12.5518956	-0.0386498
H	1.9305289	10.0918170	-0.0277121
H	-5.2665556	13.7003393	-0.0156774
H	-5.2264577	11.2386063	-0.0112962
H	-5.1968076	8.7949903	0.0013950
H	-5.2026203	6.3641757	0.0254724
C	-2.0102812	5.1394791	0.0559393
C	-3.4430871	5.1587152	0.0490072
H	-3.9843123	4.2111784	0.0646255
C	-1.3164687	3.8962389	0.0957011
C	-0.7345913	2.8265411	0.1419109
H	0.0153311	1.5198070	2.3841023
C	0.2865215	1.0229442	1.4533064
C	-0.0480117	1.5799257	0.2118845
C	0.3088917	0.8770175	-0.9544062
C	0.9782638	-0.3321184	-0.8743262
C	1.3426921	-0.8977998	0.3639921
C	0.9733343	-0.1797426	1.5186280
N	1.3015763	-0.6796452	2.8621707
O	2.2197562	-1.4581487	2.9627934
C	2.0227446	-2.1450123	0.3692653
H	1.2419676	-0.8744560	-1.7837903
C	2.5860583	-3.2197237	0.2640843
C	3.2723873	-4.4619419	0.1920171
H	5.2470486	-3.5356474	0.1950527
C	4.7049353	-4.4820441	0.1665385
O	0.6319587	-0.2625340	3.7822125
H	0.0509912	1.2944530	-1.9293651
C	4.8045958	-19.1744139	-0.0003495
C	5.4737554	-17.9423918	-0.0021466
C	4.7825367	-16.7165883	-0.0017865
C	5.4482487	-15.4826756	-0.0055588
C	3.3548830	-19.1876141	0.0017282
C	2.6418010	-17.9590373	0.0033842
C	3.3330676	-16.7318142	0.0023690
C	0.5226672	-19.2019387	0.0064846

C	1.1938949	-17.9728230	0.0067016
C	0.5023231	-16.7486671	0.0115081
H	-0.5703683	-19.2106392	0.0084419
H	-0.5907600	-16.7571002	0.0158394
H	6.5669695	-17.9328061	-0.0036371
H	6.5413733	-15.4706104	-0.0110461
C	4.8402076	-24.0879609	0.0007046
C	2.6972634	-25.3232721	0.0042443
C	3.3908660	-24.0984279	0.0025663
C	1.2478213	-25.3338540	0.0060645
C	0.5588175	-24.1089809	0.0059671
H	-0.5342508	-24.1167569	0.0073237
C	5.5118467	-22.8577622	-0.0005493
C	4.8231120	-21.6315624	0.0001421
C	5.4939612	-20.4007610	-0.0008013
C	2.6802996	-22.8683611	0.0029313
C	3.3735800	-21.6431000	0.0018543
C	2.6622421	-20.4135300	0.0026721
C	1.2310246	-22.8793323	0.0046452
C	0.5415858	-21.6552002	0.0053205
C	1.2133508	-20.4254566	0.0046493
H	-0.5515193	-21.6634834	0.0068202
H	6.6049881	-22.8507485	-0.0019299
H	6.5871496	-20.3926732	-0.0019565
C	-3.5726289	19.8646834	0.0106083
C	-4.2381528	18.6310502	0.0048530
C	-3.5436405	17.4075710	-0.0025201
C	-4.2069923	16.1727509	-0.0089791
C	-2.1230482	19.8817944	0.0109815
C	-1.4064522	18.6549274	0.0043972
C	-2.0941514	17.4257404	-0.0034345
C	0.7086299	19.9041488	0.0136741
C	0.0415330	18.6721867	0.0049132
C	0.7364617	17.4491575	-0.0051802
H	1.8017801	19.9162756	0.0155114
H	1.8296297	17.4614708	-0.0058760
H	-5.3311886	18.6182464	0.0052598
H	-5.3000339	16.1580910	-0.0073950
C	-3.6261238	24.7778859	0.0200265
C	-1.4880804	26.0211172	0.0222503
C	-2.1767792	24.7933563	0.0212641
C	-0.0385791	26.0369827	0.0235803
C	0.6550412	24.8141403	0.0239335
H	1.7482002	24.8260551	0.0248543
C	-4.2929931	23.5451451	0.0189071
C	-3.5996971	22.3214849	0.0178911
C	-4.2661795	21.0885171	0.0149285
C	-1.4615598	23.5655191	0.0211794
C	-2.1502145	22.3376002	0.0189070
C	-1.4346454	21.1100300	0.0163723
C	-0.0122162	23.5814144	0.0226817
C	0.6815373	22.3590078	0.0220736
C	0.0142884	21.1263016	0.0180567
H	1.7747051	22.3708838	0.0234515

H	-5.3860122	23.5335789	0.0179963
H	-5.3592071	21.0766749	0.0147130
C	4.8911852	-31.4523767	0.0074468
C	5.5629083	-30.2250395	0.0052589
C	4.8738657	-28.9983786	0.0049955
C	5.5457505	-27.7692713	0.0026460
C	4.8569090	-26.5435567	0.0023940
C	5.5288770	-25.3138317	0.0004456
C	2.7498935	-32.6871625	0.0118026
C	3.4437400	-31.4616790	0.0097759
C	2.7317883	-30.2325714	0.0097115
C	3.4254510	-29.0078025	0.0072039
C	2.7142107	-27.7780347	0.0067761
C	3.4079177	-26.5533696	0.0044251
C	1.3004847	-32.6982935	0.0142836
C	0.6107998	-31.4731446	0.0145778
C	1.2822480	-30.2434260	0.0120845
C	0.5929115	-29.0180864	0.0115749
C	1.2647038	-27.7886599	0.0088651
C	0.5757165	-26.5633542	0.0082033
H	-0.4823318	-31.4814640	0.0164868
H	-0.5001734	-29.0260047	0.0132986
H	-0.5173754	-26.5708959	0.0096356
H	6.6559672	-30.2170144	0.0035633
H	6.6388159	-27.7615931	0.0010890
H	6.6219472	-25.3067035	-0.0010550
C	4.9260800	-36.3576124	0.0087482
C	5.5977636	-35.1416437	0.0079521
C	4.9086847	-33.9056432	0.0088164
C	5.5803229	-32.6821315	0.0072403
C	3.4812754	-36.3682271	0.0108453
C	2.7681561	-35.1417558	0.0122733
C	3.4625182	-33.9150963	0.0111144
C	0.6491870	-36.3857376	0.0149543
C	1.3196523	-35.1530577	0.0145654
C	0.6293402	-33.9287997	0.0158593
H	-0.4440105	-36.3952472	0.0165427
H	-0.4638080	-33.9375189	0.0177140
H	6.6910855	-35.1339196	0.0063409
H	6.6734922	-32.6741521	0.0055082
H	5.5040455	-42.1987914	0.0042150
C	4.9618250	-41.2496182	0.0054795
H	3.3595835	-43.4298058	0.0038352
C	2.8114277	-42.4841726	0.0054803
C	3.5199593	-41.2897837	0.0064961
H	0.8697119	-43.4469811	0.0054479
C	1.4001753	-42.4919008	0.0064574
C	0.6910006	-41.3147130	0.0086690
H	-0.4018819	-41.3239356	0.0094565
C	5.6372036	-40.0740731	0.0059936
C	4.9451609	-38.8089412	0.0075494
C	5.6149807	-37.6044844	0.0074111
C	2.8030769	-40.0480613	0.0085538
C	3.4995362	-38.8238246	0.0091134

C	2.7865363	-37.5958927	0.0110200
C	1.3636797	-40.0578215	0.0098787
C	0.6707537	-38.8453657	0.0122177
C	1.3410814	-37.6067989	0.0129004
H	-0.4225572	-38.8556262	0.0133866
H	6.7301945	-40.0633037	0.0051472
H	6.7084232	-37.5966900	0.0060593
C	-3.7059113	32.1443513	0.0306057
C	-4.3727272	30.9139881	0.0256021
C	-3.6791819	29.6894543	0.0233843
C	-4.3459995	28.4573019	0.0208555
C	-3.6525347	27.2338799	0.0206947
C	-4.3194602	26.0012715	0.0197271
C	-1.5694098	33.3875598	0.0375766
C	-2.2584579	32.1590896	0.0318328
C	-1.5419561	30.9321486	0.0282627
C	-2.2307266	29.7042809	0.0248198
C	-1.5147961	28.4766811	0.0236508
C	-2.2034974	27.2489532	0.0220634
C	-0.1200268	33.4040996	0.0382447
C	0.5742150	32.1811232	0.0334363
C	-0.0924006	30.9484374	0.0292614
C	0.6015730	29.7252278	0.0269917
C	-0.0652475	28.4927141	0.0248897
C	0.6284863	27.2695678	0.0246128
H	1.6673814	32.1935260	0.0339985
H	1.6947472	29.7374756	0.0277578
H	1.7216626	27.2815953	0.0257204
H	-5.4657700	30.9017836	0.0244873
H	-5.4390069	28.4452208	0.0196955
H	-5.4124473	25.9894790	0.0188485
C	-3.7590742	37.0509613	0.0582123
C	-4.4259505	35.8321291	0.0502409
C	-3.7325379	34.5983387	0.0429018
C	-4.3994332	33.3719836	0.0356631
C	-2.3142922	37.0670091	0.0582799
C	-1.5968640	35.8427649	0.0509573
C	-2.2864469	34.6132408	0.0436388
C	0.5173342	37.0949445	0.0585956
C	-0.1484237	35.8594745	0.0512690
C	0.5463789	34.6374339	0.0445348
H	1.6105176	37.1085100	0.0586780
H	1.6395470	34.6501225	0.0448709
H	-5.5191366	35.8204826	0.0498206
H	-5.4925275	33.3599251	0.0348702
H	-4.3595480	42.8900767	0.0889711
C	-3.8138053	41.9428980	0.0844275
H	-2.2203480	44.1295637	0.0935080
C	-1.6684138	43.1860209	0.0893150
C	-2.3720733	41.9887162	0.0842016
H	0.2693663	44.1569020	0.0931171
C	-0.2572339	43.1994965	0.0891097
C	0.4566755	42.0250448	0.0839251
H	1.5494771	42.0394396	0.0838366

C	-4.4845494	40.7648046	0.0791322
C	-3.7874818	39.5023214	0.0725459
C	-4.4526090	38.2953282	0.0660228
C	-1.6502740	40.7497457	0.0783432
C	-2.3419409	39.5227513	0.0723265
C	-1.6242375	38.2973972	0.0655695
C	-0.2108963	40.7651786	0.0782850
C	0.4865738	39.5551778	0.0723944
C	-0.1788325	38.3138098	0.0656774
H	1.5798126	39.5696710	0.0725522
H	-5.5775143	40.7499102	0.0794028
H	-5.5460239	38.2836285	0.0663428

Table S3: xyz coordinates for the lead dimer (in Å)

C	-1.7751522	-0.6271928	0.0000000
C	-0.3257249	-0.6164673	0.0000000
C	2.5060840	-0.6061770	0.0000000
H	3.5992455	-0.5985656	0.0000000
H	-3.5398783	-1.8659316	0.0000000
C	-2.4466657	-1.8577369	0.0000000
C	0.3851855	-1.8468092	0.0000000
C	1.8346743	-1.8365300	0.0000000
C	-1.7572947	-3.0831308	0.0000000
C	-0.3077748	-3.0723866	0.0000000
C	2.5237778	-3.0622804	0.0000000
H	3.6168619	-3.0539096	0.0000000
H	-3.5218549	-4.3211435	0.0000000
C	-2.4286612	-4.3134022	0.0000000
C	0.4035073	-4.3026174	0.0000000
C	1.8526711	-4.2926252	0.0000000
C	-1.7390491	-5.5388924	0.0000000
C	-0.2894602	-5.5280293	0.0000000
C	2.5420011	-5.5183436	0.0000000
H	3.6350843	-5.5098618	0.0000000
H	-3.5029972	-6.7778078	0.0000000
C	-2.4098896	-6.7691601	0.0000000
C	0.4223109	-6.7579391	0.0000000
C	1.8709206	-6.7482167	0.0000000
C	-1.7202256	-7.9946391	0.0000000
C	-0.2706606	-7.9835411	0.0000000
C	2.5602495	-7.9751296	0.0000000
H	3.6534165	-7.9666327	0.0000000
H	-3.4842391	-9.2337270	0.0000000
C	-2.3911120	-9.2249640	0.0000000
C	0.4415603	-9.2128580	0.0000000
C	1.8891621	-9.2032720	0.0000000
C	-1.7011929	-10.4502140	0.0000000
C	-0.2518133	-10.4389047	0.0000000
C	2.5782382	-10.4334390	0.0000000
H	3.6714445	-10.4251795	0.0000000
H	-3.4650912	-11.6900335	0.0000000
C	-2.3719607	-11.6810596	0.0000000

C	0.4608369	-11.6671048	0.0000000
C	1.9069781	-11.6574436	0.0000000
C	-1.6815821	-12.9053875	0.0000000
C	-0.2331429	-12.8940833	0.0000000
C	2.5958960	-12.8937513	0.0000000
H	3.6891486	-12.8860011	0.0000000
H	-3.4450828	-14.1481261	0.0000000
C	-2.3519582	-14.1381793	0.0000000
C	0.4797691	-14.1208493	0.0000000
C	1.9245737	-14.1102346	0.0000000
C	-1.6604249	-15.3594211	0.0000000
C	-0.2149700	-15.3485150	0.0000000
C	2.6134744	-15.3571067	0.0000000
H	3.7069169	-15.3493122	0.0000000
H	-3.4240634	-16.6082484	0.0000000
C	-2.3307526	-16.5979879	0.0000000
C	0.4980299	-16.5764468	0.0000000
C	1.9436546	-16.5615634	0.0000000
C	-1.6378266	-17.8104438	0.0000000
C	-0.1984294	-17.8006836	0.0000000
H	-2.1317943	-21.1996034	0.0000000
C	-1.6013310	-20.2445230	0.0000000
C	-0.1900785	-20.2367949	0.0000000
H	0.3580773	-21.1824280	0.0000000
H	2.5025392	-19.9514137	0.0000000
H	-3.4033882	-19.0765579	0.0000000
C	-2.3105056	-19.0673352	0.0000000
C	0.5184530	-19.0424059	0.0000000
C	1.9603188	-19.0022404	0.0000000
C	2.6356973	-17.8266953	0.0000000
H	3.7286882	-17.8159260	0.0000000
C	1.7751522	0.6271928	0.0000000
C	0.3257249	0.6164673	0.0000000
C	-2.5060840	0.6061770	0.0000000
H	-3.5992455	0.5985656	0.0000000
H	3.5398783	1.8659316	0.0000000
C	2.4466657	1.8577369	0.0000000
C	-0.3851855	1.8468092	0.0000000
C	-1.8346743	1.8365300	0.0000000
C	1.7572947	3.0831308	0.0000000
C	0.3077748	3.0723866	0.0000000
C	-2.5237778	3.0622804	0.0000000
H	-3.6168619	3.0539096	0.0000000
H	3.5218549	4.3211435	0.0000000
C	2.4286612	4.3134022	0.0000000
C	-0.4035073	4.3026174	0.0000000
C	-1.8526711	4.2926252	0.0000000
C	1.7390491	5.5388924	0.0000000
C	0.2894602	5.5280293	0.0000000
C	-2.5420011	5.5183436	0.0000000
H	-3.6350843	5.5098618	0.0000000
H	3.5029972	6.7778078	0.0000000
C	2.4098896	6.7691601	0.0000000
C	-0.4223109	6.7579391	0.0000000

C	-1.8709206	6.7482167	0.0000000
C	1.7202256	7.9946391	0.0000000
C	0.2706606	7.9835411	0.0000000
C	-2.5602495	7.9751296	0.0000000
H	-3.6534165	7.9666327	0.0000000
H	3.4842391	9.2337270	0.0000000
C	2.3911120	9.2249640	0.0000000
C	-0.4415603	9.2128580	0.0000000
C	-1.8891621	9.2032720	0.0000000
C	1.7011929	10.4502140	0.0000000
C	0.2518133	10.4389047	0.0000000
C	-2.5782382	10.4334390	0.0000000
H	-3.6714445	10.4251795	0.0000000
H	3.4650912	11.6900335	0.0000000
C	2.3719607	11.6810596	0.0000000
C	-0.4608369	11.6671048	0.0000000
C	-1.9069781	11.6574436	0.0000000
C	1.6815821	12.9053875	0.0000000
C	0.2331429	12.8940833	0.0000000
C	-2.5958960	12.8937513	0.0000000
H	-3.6891486	12.8860011	0.0000000
H	3.4450828	14.1481261	0.0000000
C	2.3519582	14.1381793	0.0000000
C	-0.4797691	14.1208493	0.0000000
C	-1.9245737	14.1102346	0.0000000
C	1.6604249	15.3594211	0.0000000
C	0.2149700	15.3485150	0.0000000
C	-2.6134744	15.3571067	0.0000000
H	-3.7069169	15.3493122	0.0000000
H	3.4240634	16.6082484	0.0000000
C	2.3307526	16.5979879	0.0000000
C	-0.4980299	16.5764468	0.0000000
C	-1.9436546	16.5615634	0.0000000
C	1.6378266	17.8104438	0.0000000
C	0.1984294	17.8006836	0.0000000
H	2.1317943	21.1996034	0.0000000
C	1.6013310	20.2445230	0.0000000
C	0.1900785	20.2367949	0.0000000
H	-0.3580773	21.1824280	0.0000000
H	-2.5025392	19.9514137	0.0000000
H	3.4033882	19.0765579	0.0000000
C	2.3105056	19.0673352	0.0000000
C	-0.5184530	19.0424059	0.0000000
C	-1.9603188	19.0022404	0.0000000
C	-2.6356973	17.8266953	0.0000000
H	-3.7286882	17.8159260	0.0000000

References

(S1) Chen, L.; Hansen, T.; Franco, I. *J. Phys. Chem. C* **2014**, *118*, 20009–20017.

(S2) Zelovich, T.; Kronik, L.; Hod, O. *J. Phys. Chem. C* **2016**, *120*, 15052–15062.

(S3) Zelovich, T.; Hansen, T.; Liu, Z.-F.; Neaton, J. B.; Kronik, L.; Hod, O. *J. Chem. Phys.* **2017**, *146*, 092331.

(S4) Zelovich, T.; Kronik, L.; Hod, O. *J. Chem. Theory Comput.* **2014**, *10*, 2927–2941.

(S5) Zelovich, T.; Kronik, L.; Hod, O. *J. Chem. Theory Comput.* **2015**, *11*, 4861–4869.

(S6) Hod, O.; Rodríguez-Rosario, C. A.; Zelovich, T.; Frauenheim, T. *J. Phys. Chem. A* **2016**, *120*, 3278–3285.

(S7) Henderson, T. M.; Fagas, G.; Hyde, E.; Greer, J. C. *J. Chem. Phys.* **2006**, *125*, 244104.

(S8) Liu, Z.-F.; Neaton, J. B. *J. Chem. Phys.* **2014**, *141*, 131104.

(S9) Hod, O.; Peralta, J. E.; Scuseria, G. E. *J. Chem. Phys.* **2006**, *125*, 114704.

(S10) Nafie, L. A. *J. Phys. Chem. A* **1997**, *101*, 7826.

(S11) Pohl, V.; Hermann, G.; Tremblay, J. C. *J. Comput. Chem.* **2017**, *38*, 1515–1527.

(S12) Pohl, V.; Tremblay, J. C. *J. Phys. Chem. C* **2016**, *120*, 28808–28819.

(S13) TURBOMOLE V6.5 2013, A Development of University of Karlsruhe and Forschungszentrum Karlsruhe GmbH, 1989-2007, TURBOMOLE GmbH, since 2007; available from `http://www.turbomole.com` (accessed Dez 05, 2018).

(S14) Adamo, C.; Barone, V. *J. Chem. Phys.* **1999**, *110*, 6158–6170.

(S15) Weigend, F.; Ahlrichs, R. *Phys. Chem. Chem. Phys.* **2005**, *7*, 3297–3305.

(S16) Agapito, L. A.; Cheng, H.-P. *J. Phys. Chem. C* **2007**, *111*, 14266–14273.

(S17) Bahn, S. R.; Jacobsen, K. W. *Comput. Sci. Eng.* **2002**, *4*, 56–66.

(S18) Larsen, A. H.; Mortensen, J. J.; Blomqvist, J.; Castelli, I. E.; Christensen, R.; Dułak, M.; Friis, J.; Groves, M. N.; Hammer, B.; Hargus, C.; Hermes, E. D.; Jennings, P. C.; Jensen, P. B.; Kermode, J.; Kitchin, J. R.; Kolsbjerg, E. L.; Kubal, J.; Kaasbjerg, K.; Lysgaard, S.; Maronsson, J. B.; Maxson, T.; Olsen, T.; Pastewka, L.; Peterson, A.; Rostgaard, C.; Schiøtz, J.; Schütt, O.; Strange, M.; Thygesen, K. S.; Vegge, T.; Vilhelmsen, L.; Walter, M.; Zeng, Z.; Jacobsen, K. W. *J. Phys. Condens. Matter* **2017**, *29*, 273002.

(S19) Thygesen, K. S.; Bollinger, M. V.; Jacobsen, K. W. *Phys. Rev. B* **2003**, *67*, 115404.

(S20) Thygesen, K.; Jacobsen, K. *Chem. Phys.* **2005**, *319*, 111–125.

(S21) Strange, M.; Kristensen, I. S.; Thygesen, K. S.; Jacobsen, K. W. *J. Chem. Phys.* **2008**, *128*, 114714.

(S22) Tremblay, J. C.; Klamroth, T.; Saalfrank, P. *J. Chem. Phys.* **2008**, *129*, 084302–084309.

(S23) Tremblay, J. C.; Carrington Jr., T. *J. Chem. Phys.* **2004**, *121*, 11535–11541.

(S24) Hermann, G.; Pohl, V.; Tremblay, J. C.; Paulus, B.; Hege, H.-C.; Schild, A. *J. Comput. Chem.* **2016**, *37*, 1511–1520.

(S25) Hermann, G.; Pohl, V.; Tremblay, J. C. *J. Comput. Chem.* **2017**, *38*, 2378–2387.

(S26) Hunter, J. D. *Computing In Science & Engineering* **2007**, *9*, 90–95.

(S27) Stalling, D.; Westerhoff, M.; Hege, H.-C. *The Visualization Handbook*; Elsevier, 2005; pp 749–767.

(S28) Kokalj, A. *J. Mol. Graph. Model.* **1999**, *17*, 176–179.

(S29) Elenewski, J. E.; Gruss, D.; Zwolak, M. *J. Chem. Phys.* **2017**, *147*, 151101.